REVERSE ENGINEERING OF BIOLOGICAL STRUCTURES

Roberto Ballarini
University of Minnesota

Collaborators:

Arthur Heuer
Shekar Kamat
Hannes Kessler
Maissarath Nassirou
Liisa Kuhn
Mark Spearing
Vince Laria

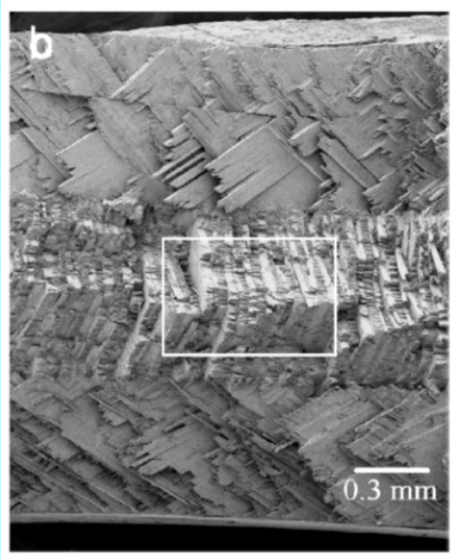

ASCE-ASME-SES
Conference on Mechanics and Materials

6/26/09

REFERENCES

“Secrets dans la Coquille,” *Pour La Science*, 2008.

“Secrets in the Shell,” *American Scientist*, 2007.

“Fracture Mechanisms of the *Strombus gigas* Conch Shell: II Micromechanics Analyses of Multiple Cracking and Large Scale Crack Bridging,” *Acta Materialia*, 2004.

“Structural Basis for the Fracture Toughness of the Shell of the Conch Strombus Gigas,” *Nature*, 2000.

“A Biomimetic Example of Brittle Toughening: Steady State Multiple Cracking,” *Computational Materials Science*, 1996.

What is an ideal composite?

It should be comprised of readily available and inexpensive materials.

It should be strong, tough and light.

It should be capable of self-healing.

It should not require prohibitive manufacturing processes.

Boeing 787 Dreamliner

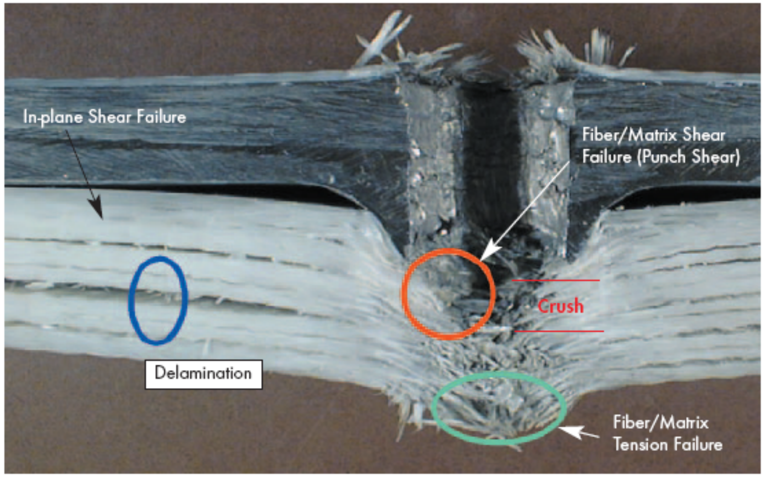

Figure 6. Damage Mechanisms Observed During the Impact and Penetration of a Composite.

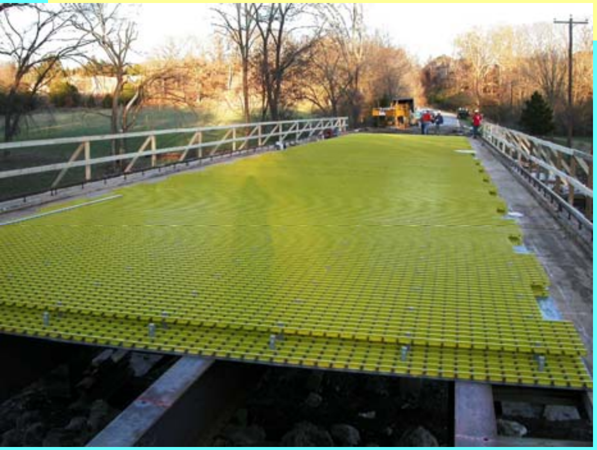

Let’s turn to *Nature* for inspiration.

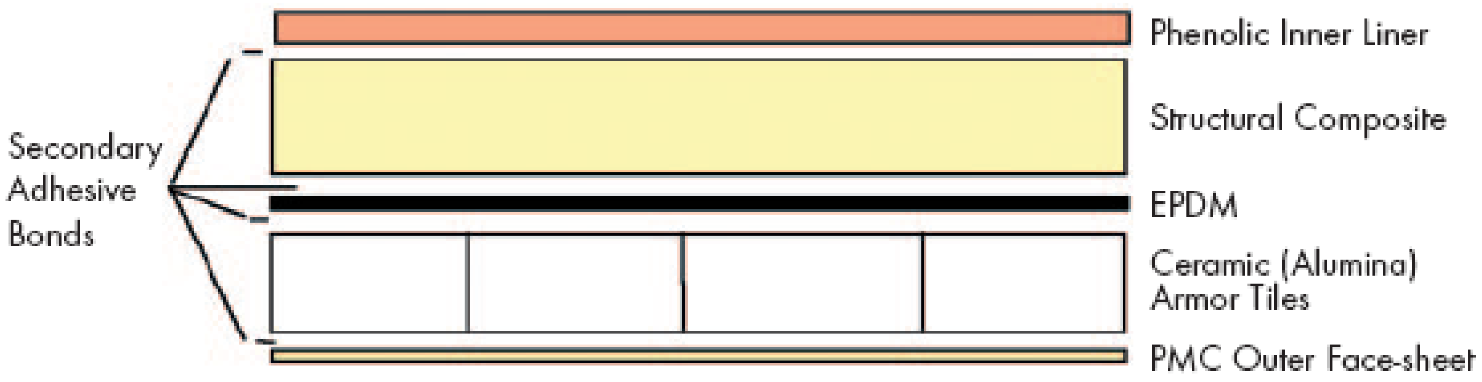

Figure 2. Example of the Composite Integral Armor Developed under the CAV Program.

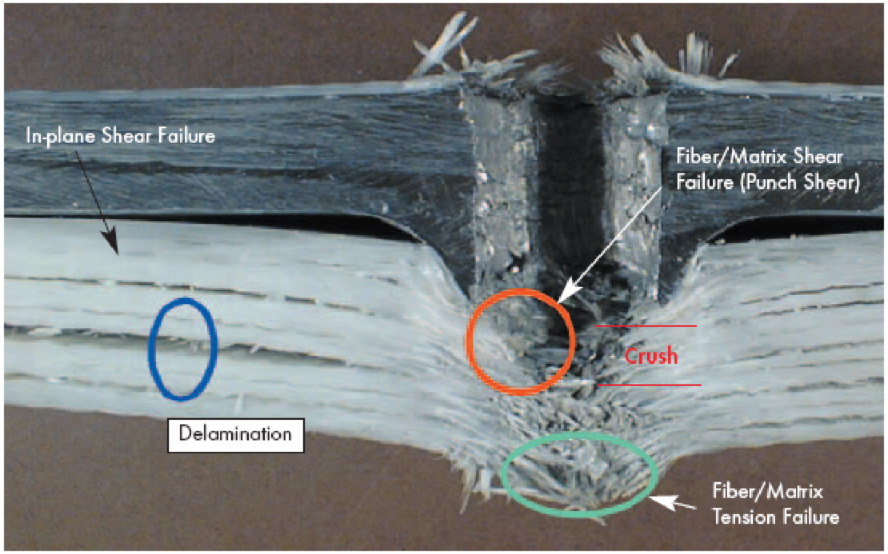

Figure 6. Damage Mechanisms Observed During the Impact and Penetration of a Composite.

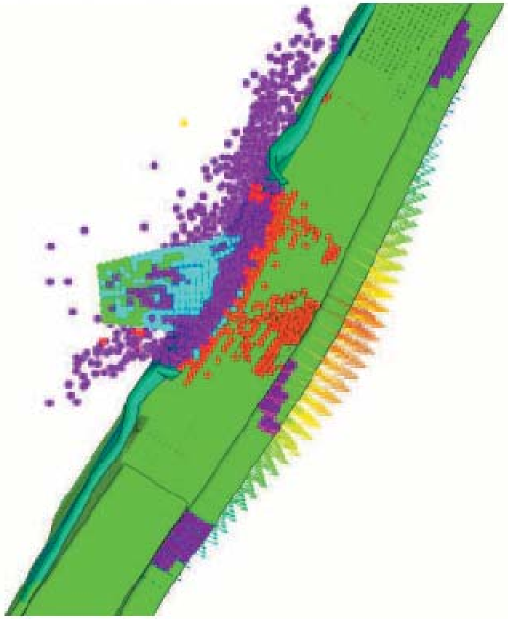

Figure 5. Modeling Ballistic Impacts into Composite Armor Has Evolved Significantly in Recent Years.

Let’s consider:

Avoiding *inappropriate* use of reductionism because it could reduce our understanding of such complex systems (as per theoretical biologist Robert Rosen).

That we may learn something by studying the biological structure despite not being able to achieve the original pie in the sky; *aim low and shoot high*.

Not using *biomimetics* in favor of *bioinspiration*.

STROMBUS GIGAS: WHY IS IT SO TOUGH?

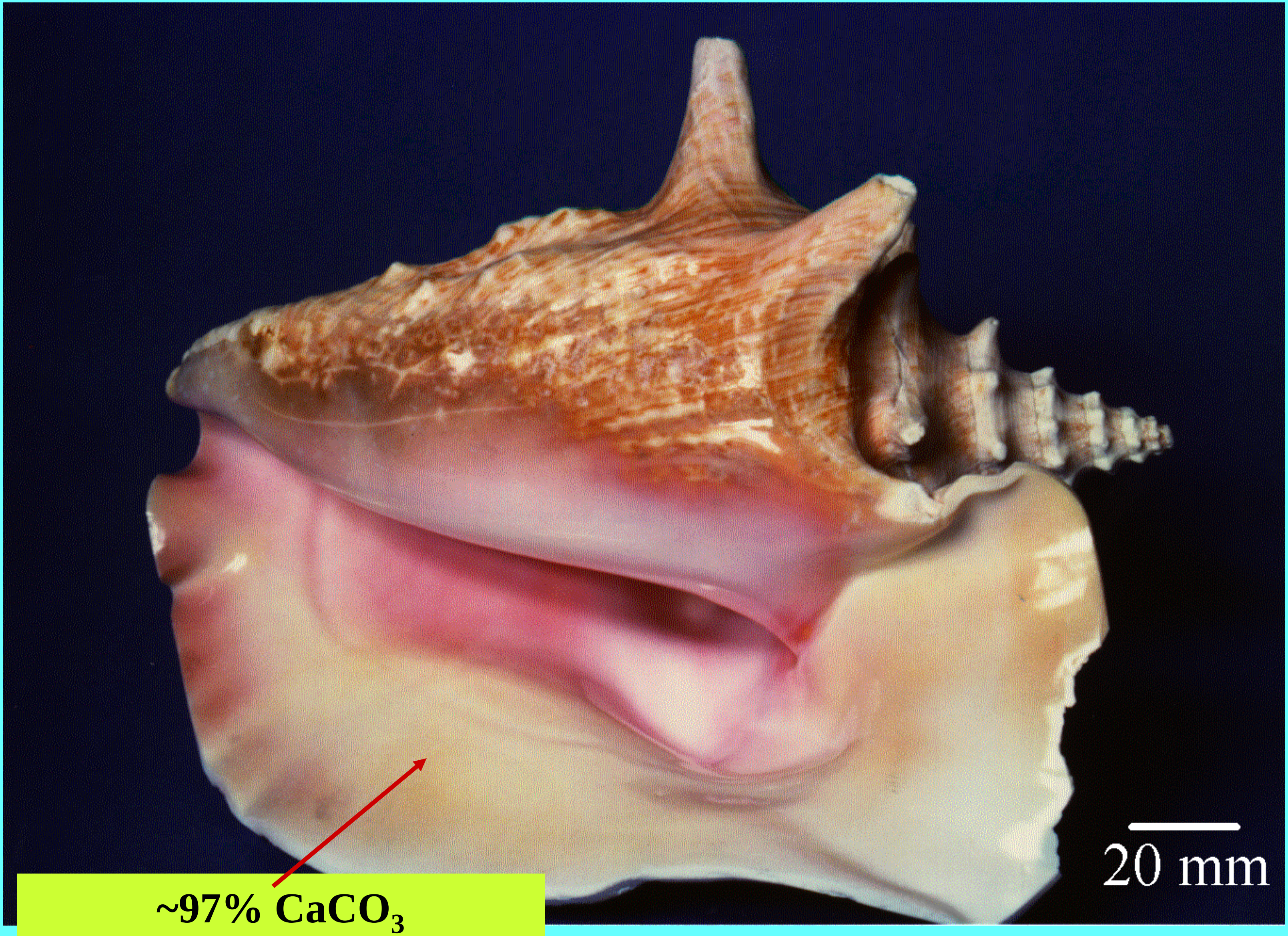

~97% $CaCO_3$
~3% protein binder

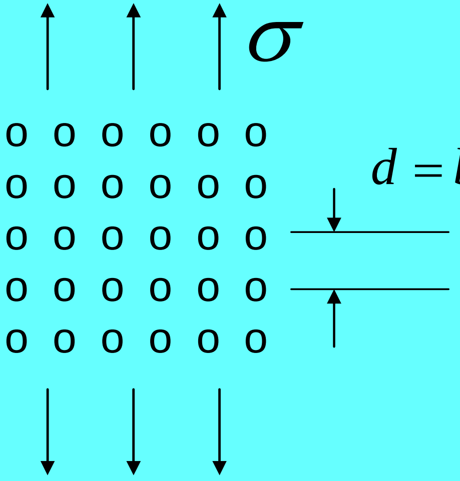

$$d = b_o + u$$

$$\sigma(x) = \frac{E}{m-n}\left[\left(\frac{b_o}{x}\right)^n - \left(\frac{b_o}{x}\right)^m\right]$$

$$\frac{2\gamma}{Eb_o} = \frac{1}{(n-1)(m-1)}$$

$$\frac{\sigma_{th}}{E} = \frac{1}{m}\left(\frac{n}{m}\right)^{n/(m-n)}$$

$$\sigma_f \approx \alpha(a/h)\sqrt{\frac{E\gamma}{a}}$$

$$\frac{\sigma_f}{\sigma_{th}} = \frac{1}{\sqrt{\pi}}\frac{m}{(n/m)^{n/(m-n)}\sqrt{(n-1)(m-1)}}\sqrt{\frac{b_o}{a}}$$

Aragonite is brittle (flaw-sensitive), but available.

Bond type	n	M	σ_{th}/E	$\sqrt{\frac{a}{b_o}}\frac{\sigma_f}{\sigma_{th}}$	$\frac{2\gamma}{Eb_o}$
Metallic	4	7	0.0677	1.96	0.0556
Ionic	2	10	0.0677	2.82	0.111
Covalent	8	12	0.0370	1.74	0.0130

PREDATORS

Spiny Lobster

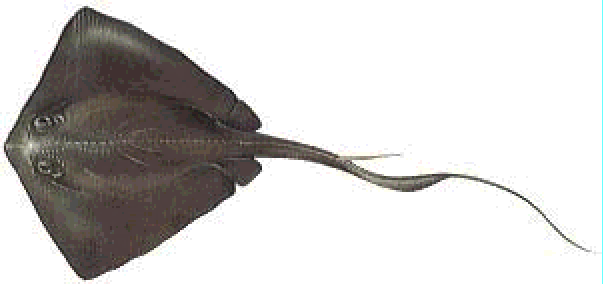

Southern Stingray

Loggerhead Turtle

Blue Crab

Octopus

Porcupine Fish


© SeaPics.com

MATERIAL SELECTION CHARTS AND MATERIAL INDICES

M. Ashby, *Materials Selection in Mechanical Design*: Pergamon, 1992

Design	Tie in tension	Beam in Flexure	Plate in Flexure
Strength to weight	σ_f / ρ	$\sigma_f^{2/3} / \rho$	$\sigma_f^{1/2} / \rho$
Stiffness to weight	E / ρ	$E^{1/2} / \rho$	$E^{1/3} / \rho$
Large recoverable deformation	σ_f / E	σ_f / E	σ_f / E
Strain energy per volume	σ_f^2 / E	σ_f^2 / E	σ_f^2 / E

Material	E GPa	ρ Mg/m^3	E/ρ GPa/Mg/m^3	$E^{1/2}/\rho$ GPa$^{1/2}$/Mg/m^3	$E^{1/3}/\rho$ GPa$^{1/2}$/Mg/m^3
Palm	**3.5**	**0.15**	**23**	**12.5**	**(10.1)**
Mild steel	**210**	**7.9**	**27**	**1.8**	**(0.8)**
Balsa wood (LD)	**2.0**	**0.1**	**20**	**14.1**	**(12.6)**

Material	σ_f MPa	ρ Mg/m^3	σ_f / ρ MPa/Mg/m^3	$\sigma_f^{2/3} / \rho$ MPa$^{2/3}$/Mg/m^3	$\sigma_f^{1/2} / \rho$ MPa$^{1/2}$/Mg/m^3
Single silk fibre	**2000**	**1.3**	**1500**	**120**	**(35)**
Single carbon fibre	**2200**	**2.0**	**1100**	**85**	**(24)**
Mild steel	**400**	**7.9**	**51**	**6.9**	**2.5**
Balsa wood (LD)	**16**	**0.1**	**160**	**64**	**(40.0)**

Material	E MPa	ρ Mg/m^3	σ_f MPa	σ_f^2/E MJ/m^3	σ_f/E
Single silk fibre	20000	1.3	1500	113	0.08
Cartilage	5	1.3	11	24.2	2.2
Skin	20	1.2	11	6.1	0.55
Leather	45	0.9	45	45.0	1.0
Spring steel	210000	7.5	2000	19.0	0.01
Soft butyl rubber	10	1.0	14	19.6	1.4

CRACK TIP PARAMETERS

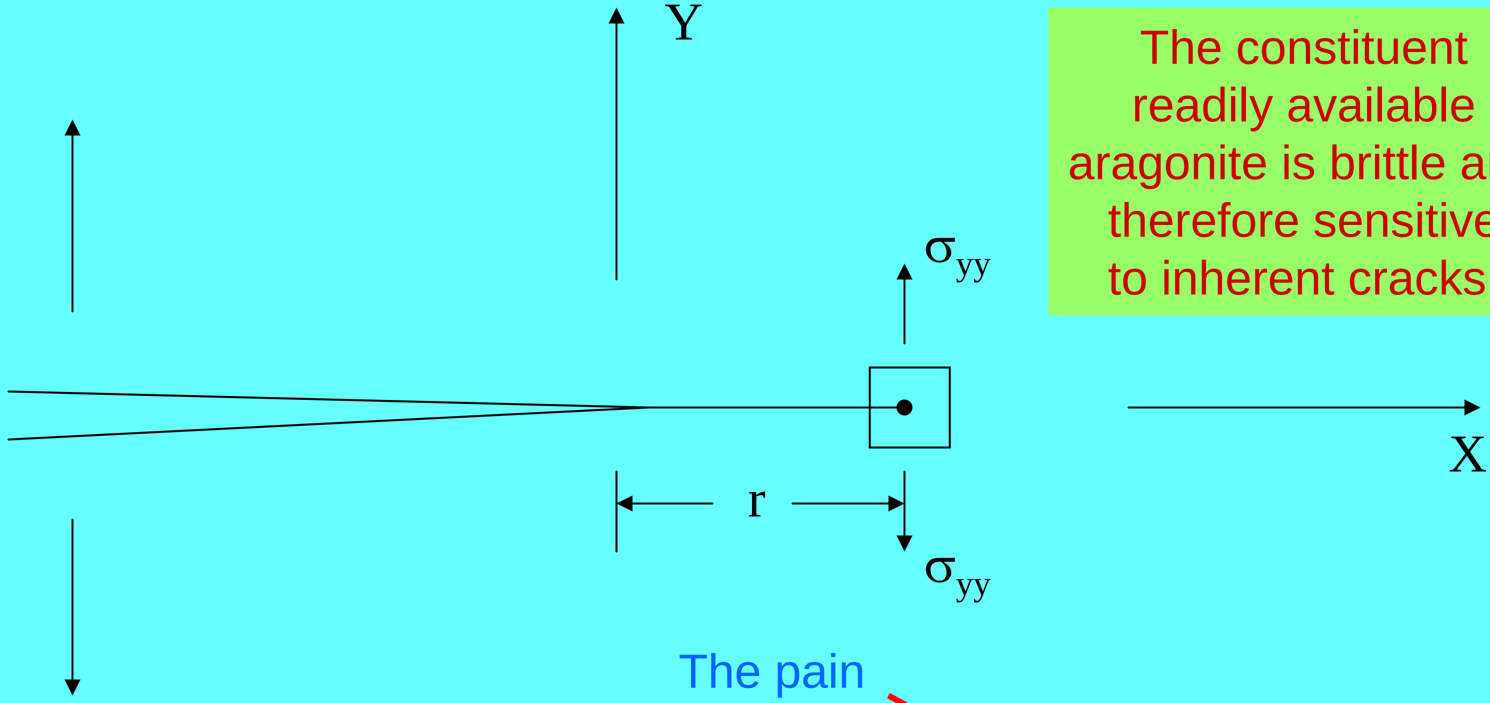

The constituent readily available aragonite is brittle and therefore sensitive to inherent cracks.

The pain felt by the material.

$$\sigma_{yy} \approx \sqrt{\frac{EJ}{r}}$$

J_c , a material property, is all the pain it can take before the crack grows.

Material	E GPa	$(EJ_c)^{1/2}$ MPa-m$^{1/2}$	J_c kJ/m^2	$(J_c/E)^{1/2}$ mm$^{1/2}$
Antler	10	7.1	5.0	0.7
Mollusc shell	60	9.5	1.5	0.4
Mild steel	210	90	40	0.4
Skin	0.01	0.4	15.0	38.7

If a material contains an inherent crack

Load carrying capacity ~ $(EJ_c)^{1/2}$

Impact energy absorption ~ J_c

Displacement capacity ~ $(J_c/E)^{1/2}$

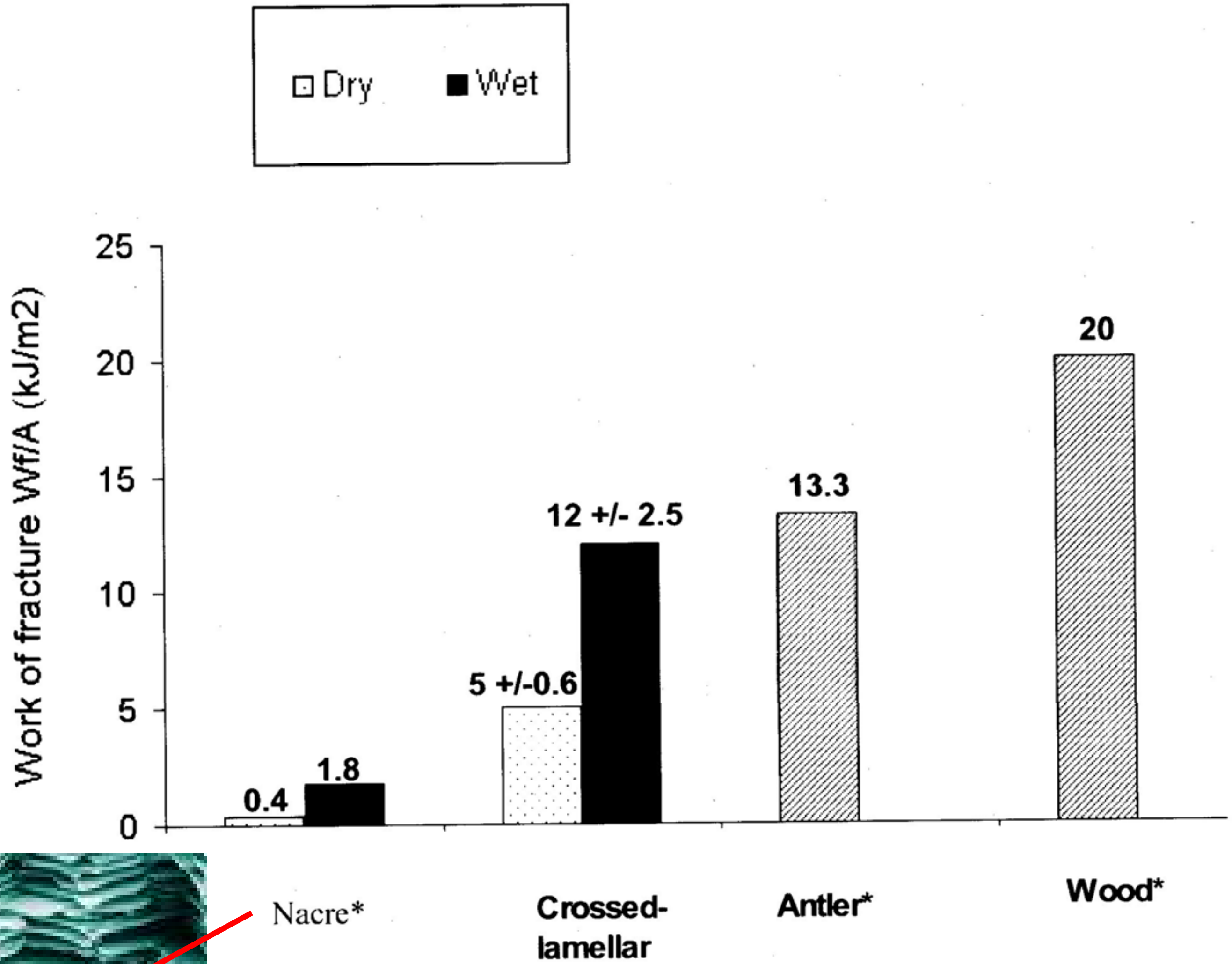

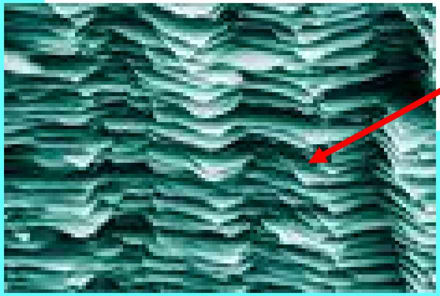

A.A.Jackson, J.F.V. Vincent and R.M. Turner (1990)
J. Mat. Sci. 25, p3137

Microstructure

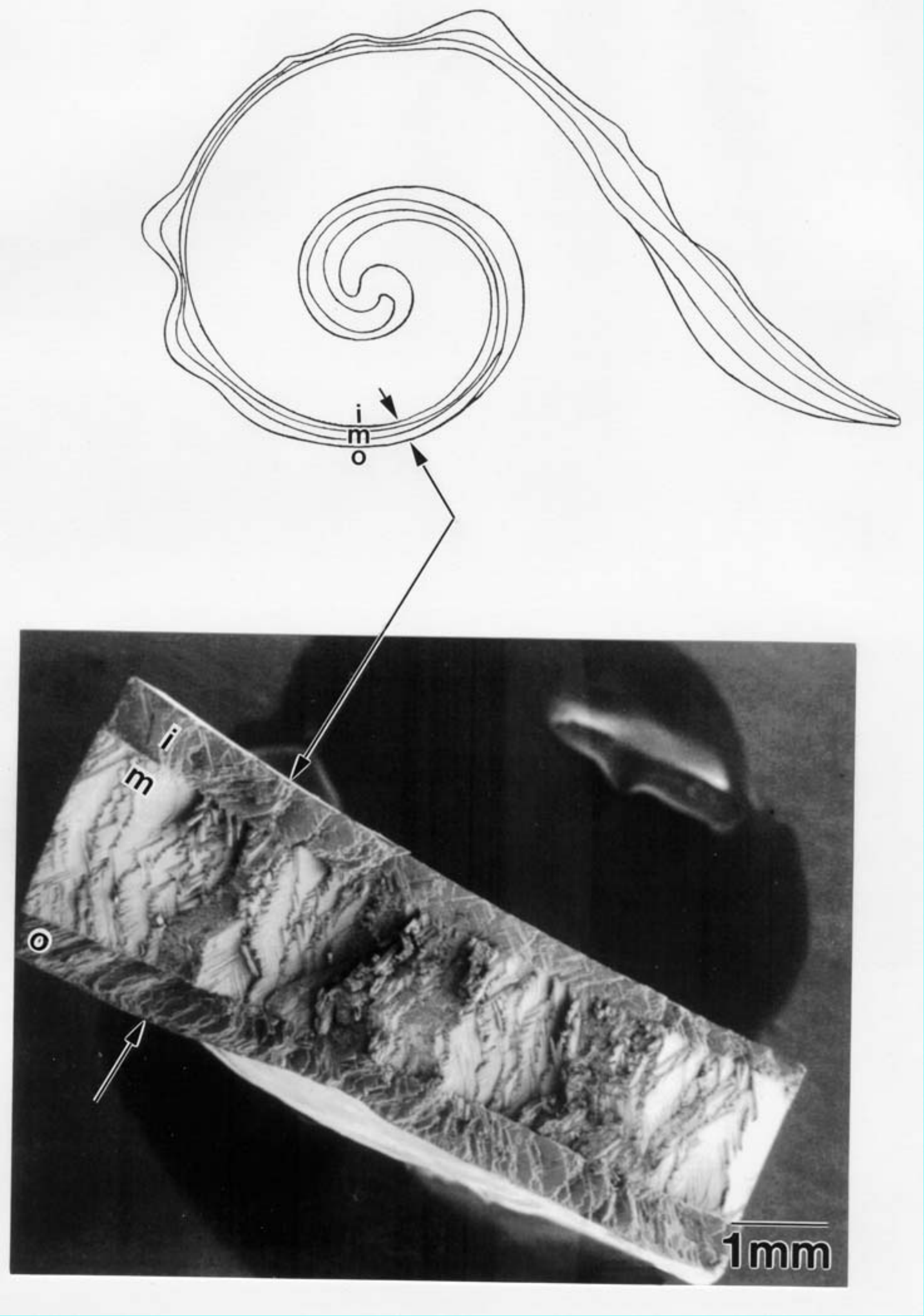

CROSSED-LAMELLAR MICROARCHITECTURE

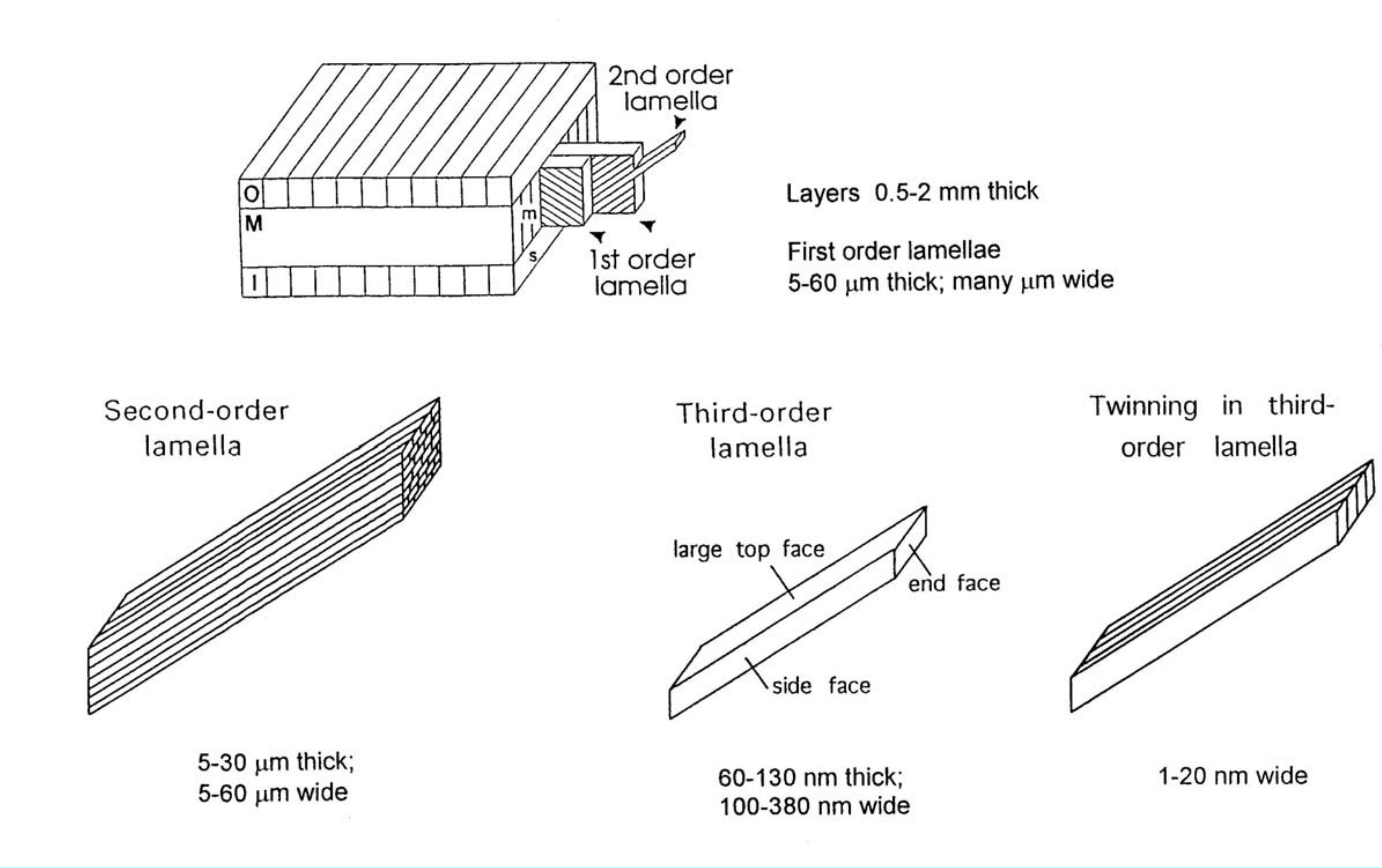

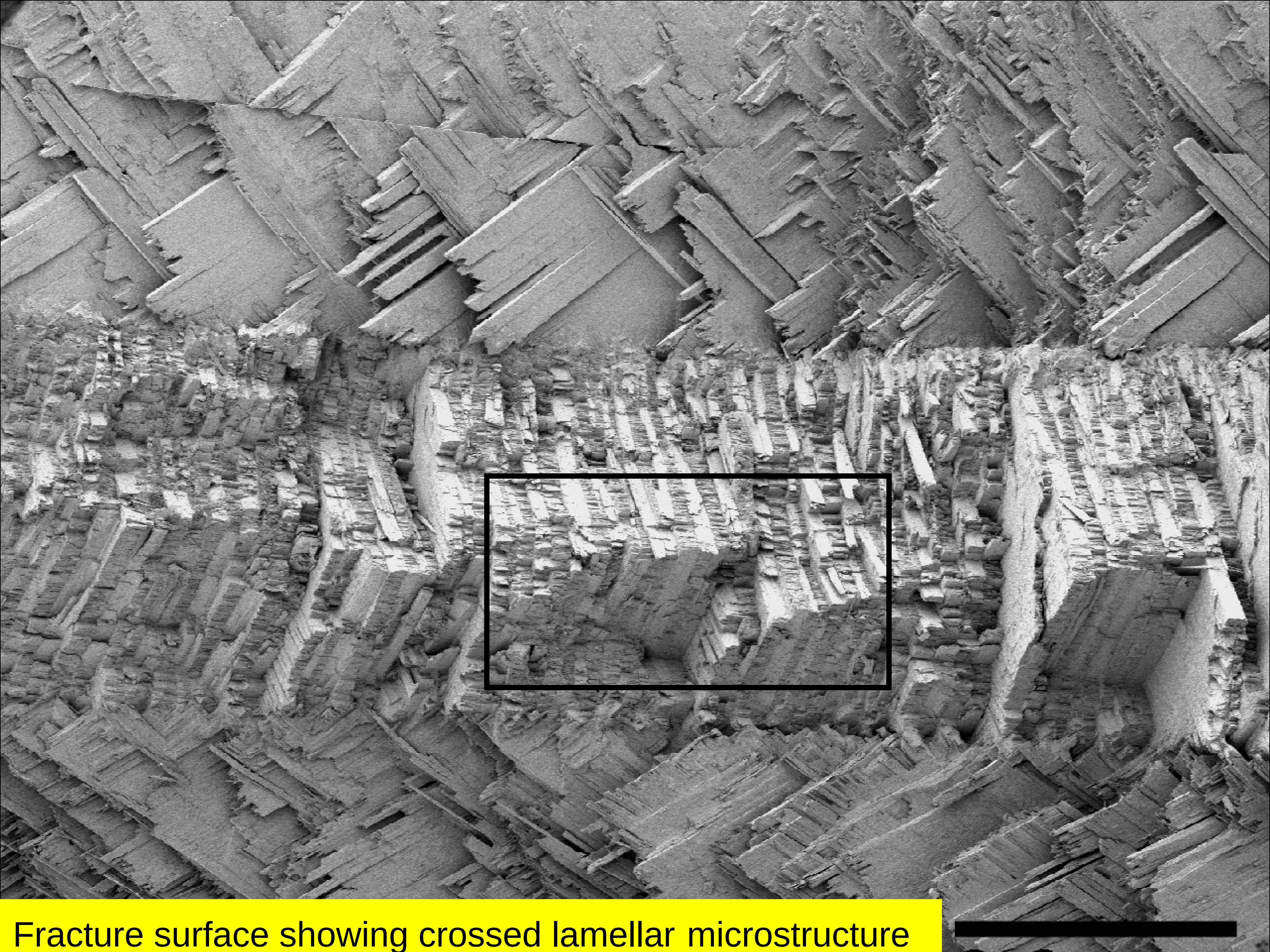

Fracture surface showing crossed lamellar microstructure

Higher Magnification SEM Images

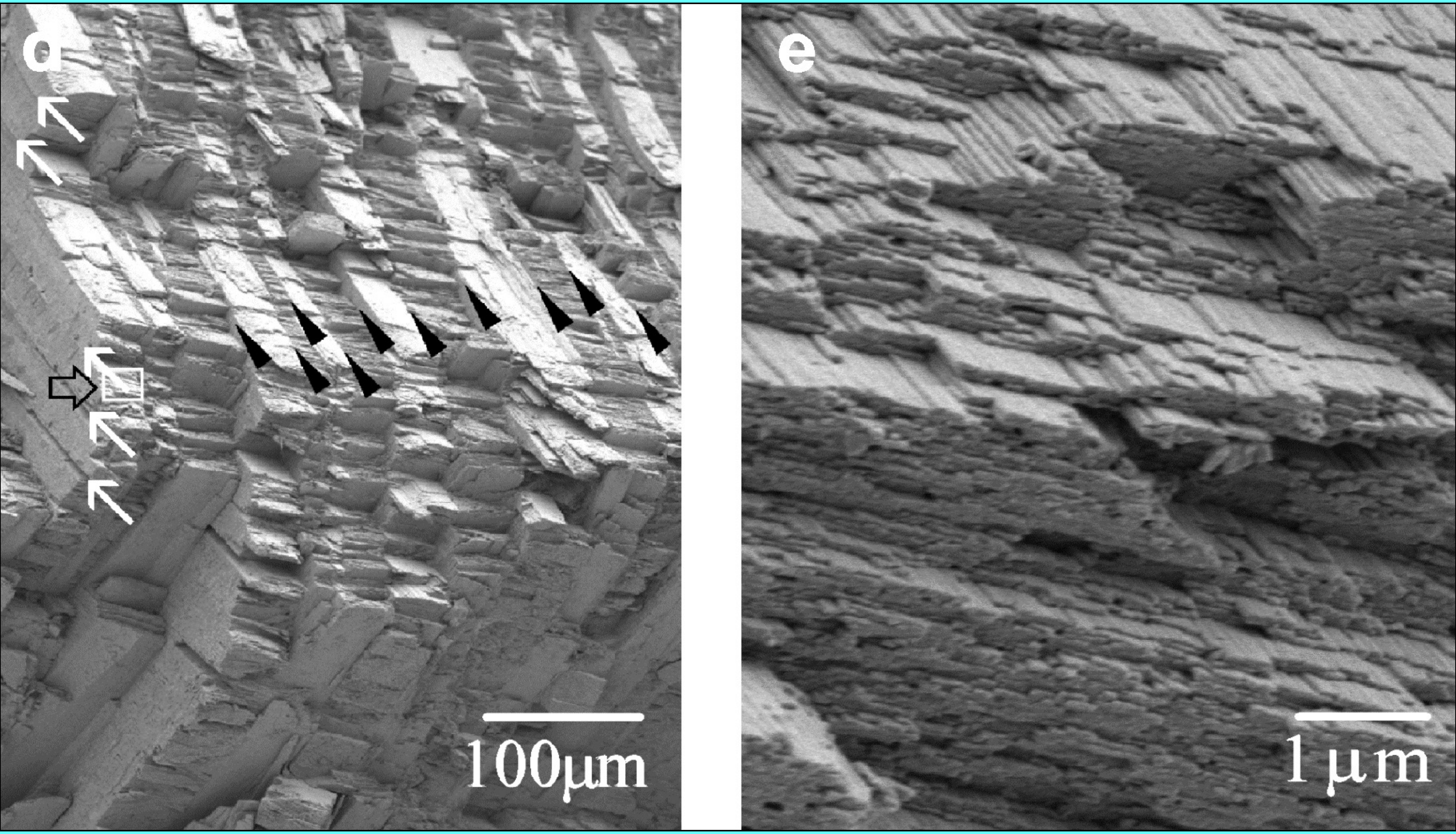

TEM MICROGRAPH OF THE INTERFACE BETWEEN SINGLE CRYSTALS OF ARAGONITE

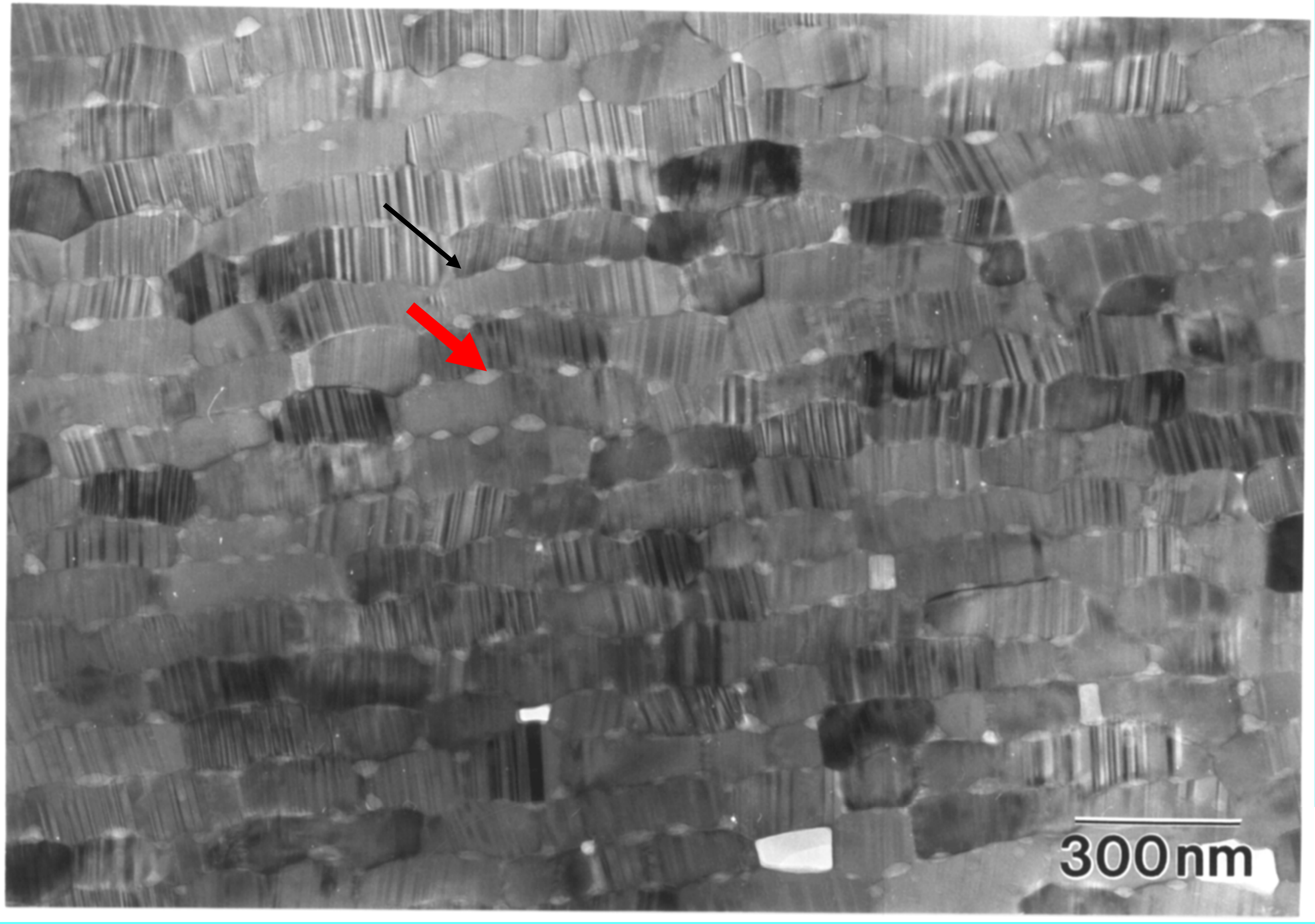

REVERSE ENGINEERING

Microstructure

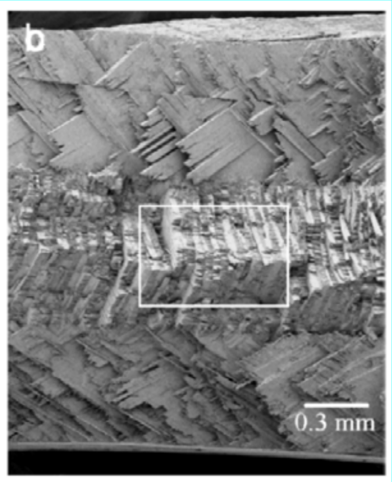

Dominant fracture mechanisms

Tunnel cracking

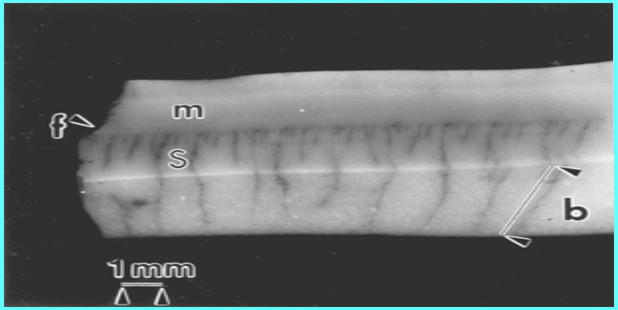

Crack bridging

Modeling

Steady-state tunneling

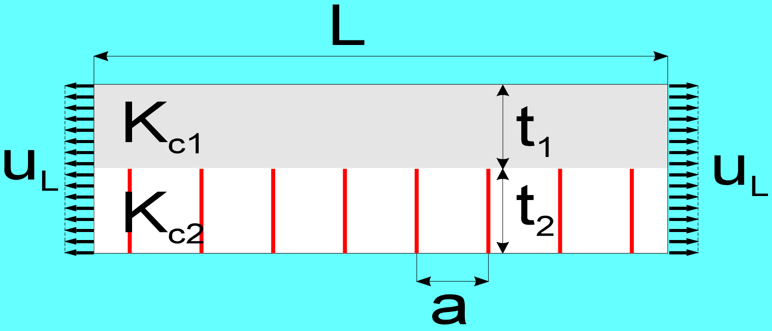

Crack bridging

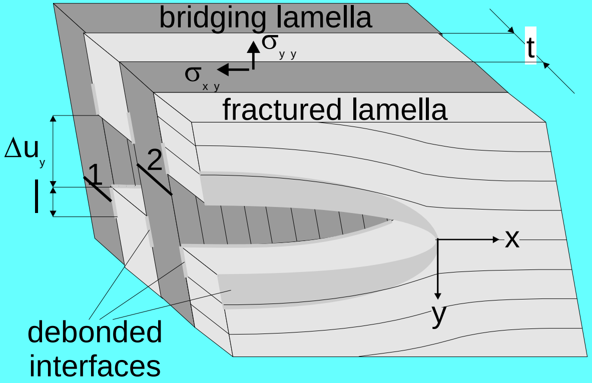

Typical Load-displacement curve of an unnotched bend bar at Room Temperature.

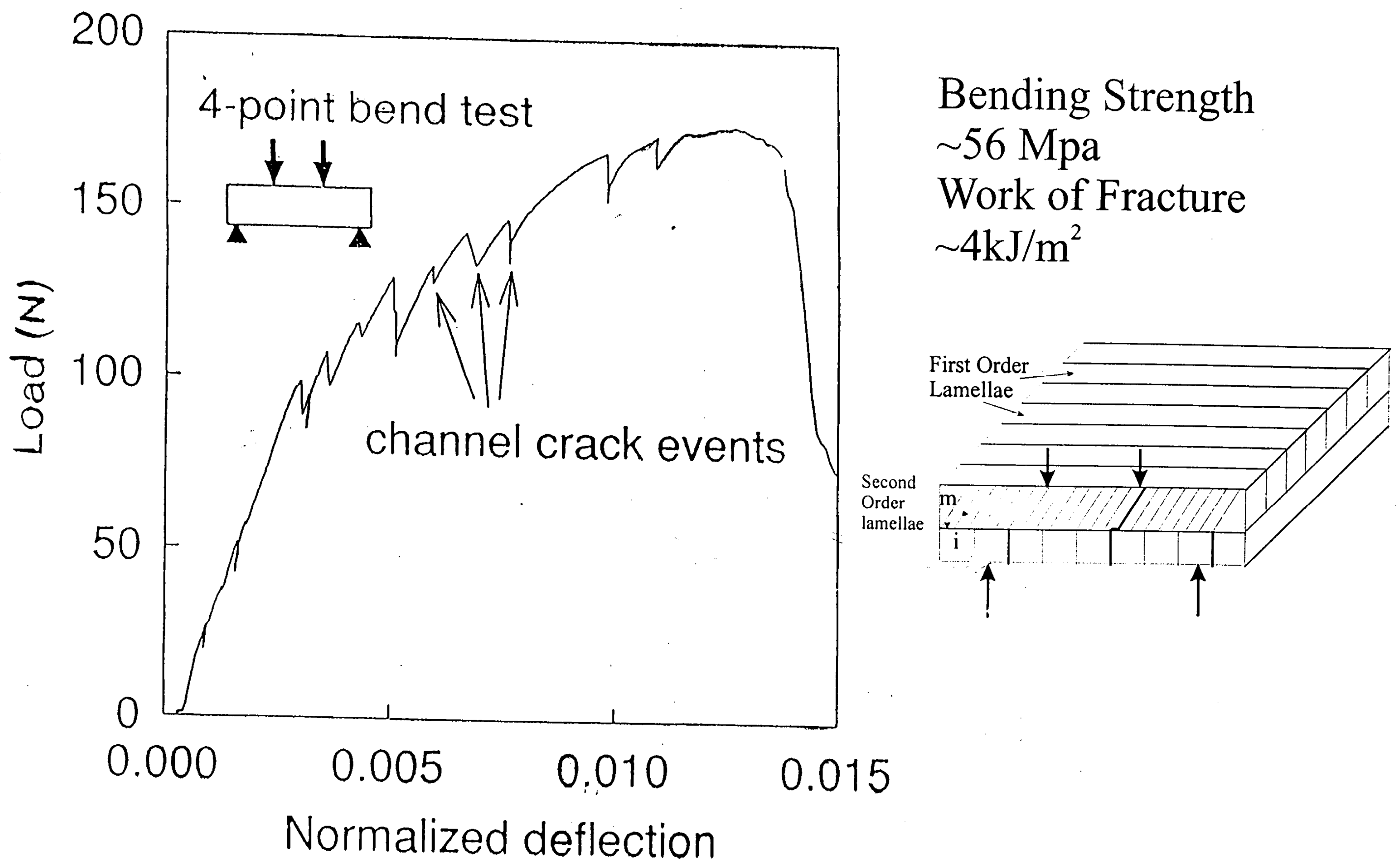

Length: 48 to 62 mm, width: 5 to 10 mm, thickness: 5 to 10 mm.

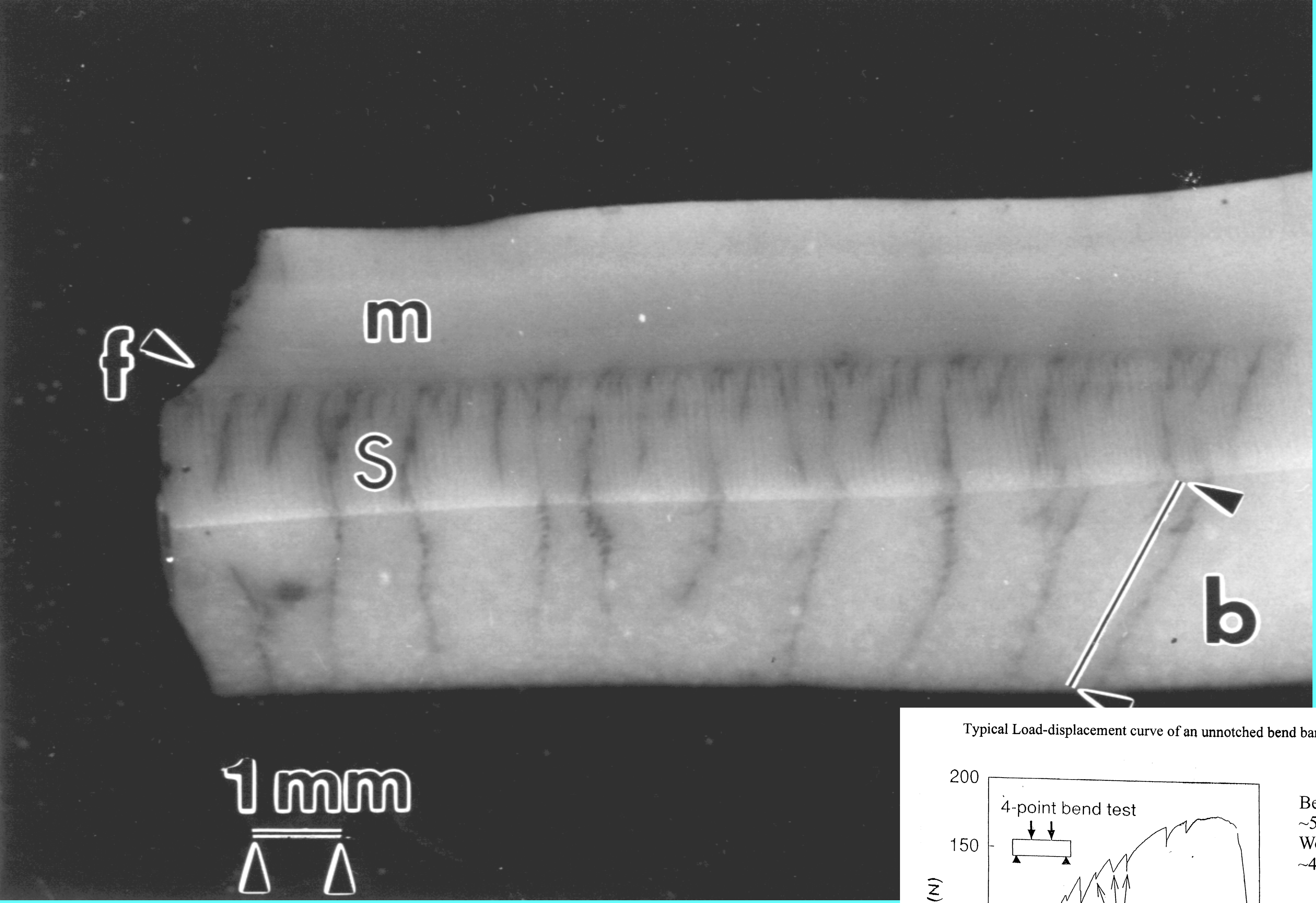

f
m
s
b
1 mm

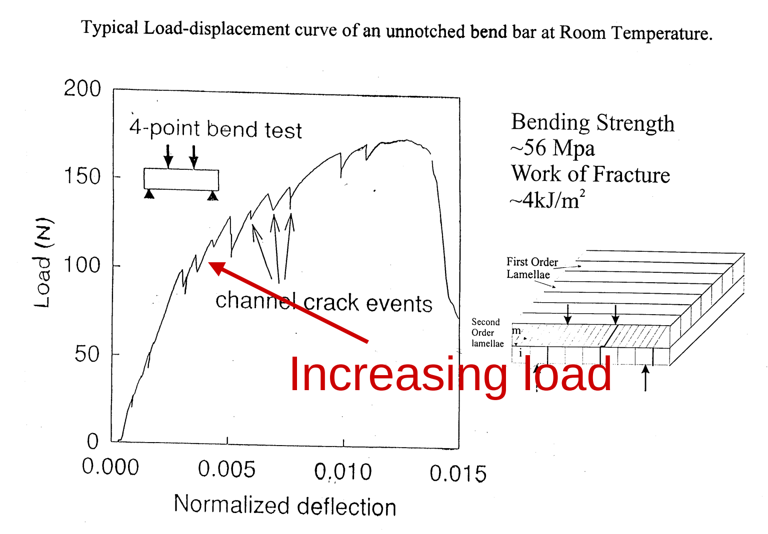

Typical Load-displacement curve of an unnotched bend bar at Room Temperature.
4-point bend test
channel crack events
Increasing load
Load (N)
Normalized deflection
200
150
100
50
0
0.000
0.005
0.010
0.015
Bending Strength
~56 Mpa
Work of Fracture
~4kJ/m2
First Order Lamellae
Second Order lamellae
m
i

IN SITU SCANNING ELECTRON MICROSCOPY

Environmental SEM

Four point bend test
Inner and outer spans:
15 and 30 mm

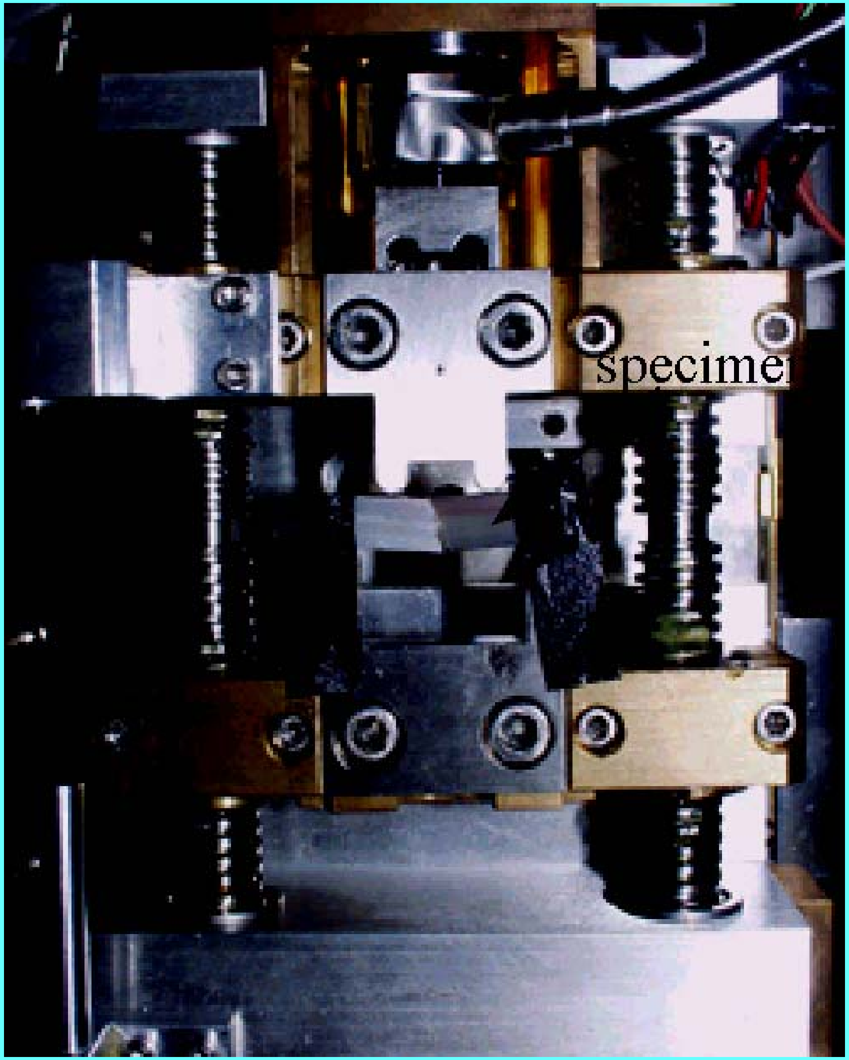

NOTCHED SAMPLE RESULTS

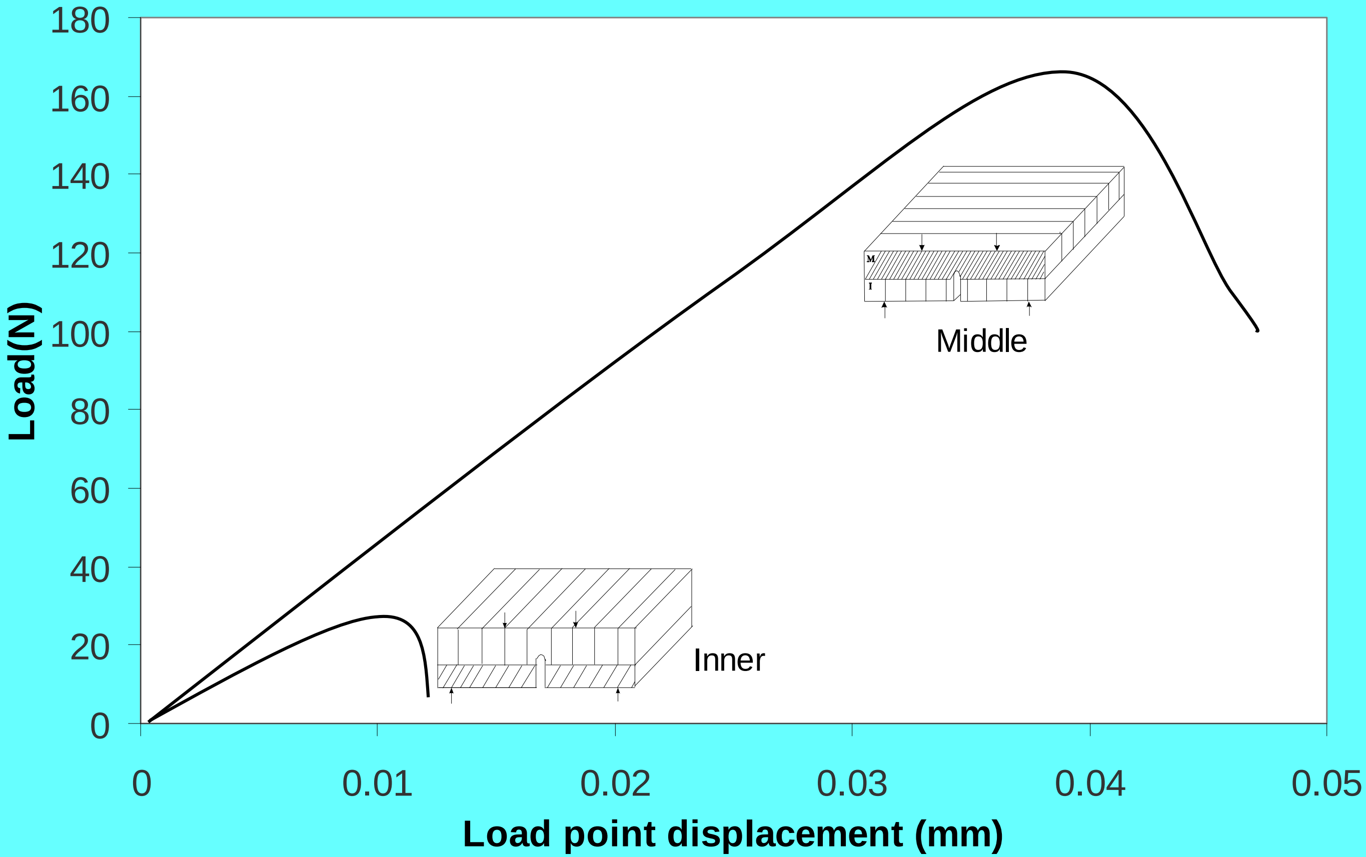

Nominal fracture toughness

inner layer: 0.46 ± 0.15 $MPa\ m^{1/2}$ ***(Use 0.6 in calculations)***

middle layer: 2.26 ± 0.77 $MPa\ m^{1/2}$

Show video

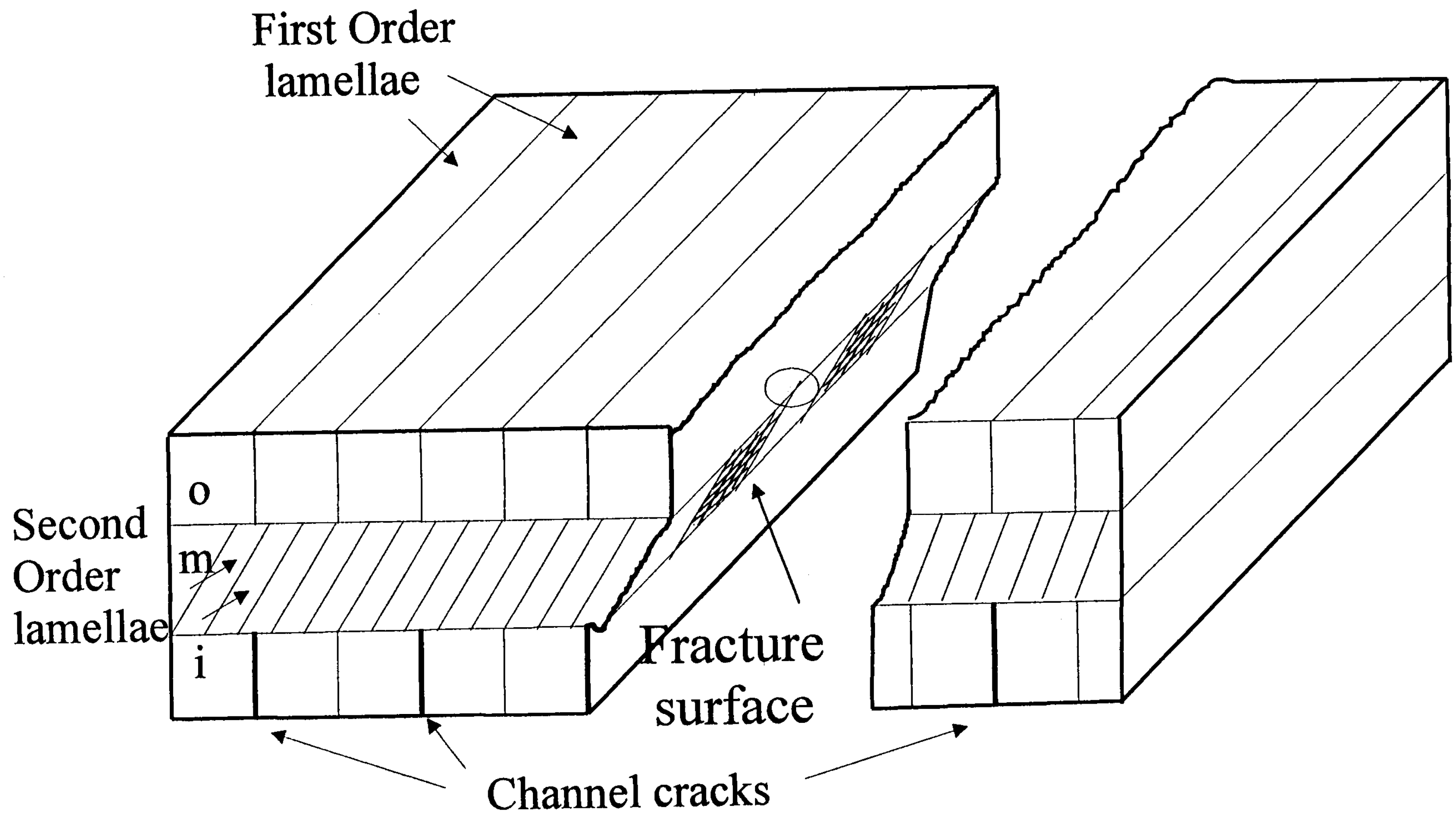
First Order
lamellae
o
Second
Order
lamellae
m
i
Fracture
surface
Channel cracks

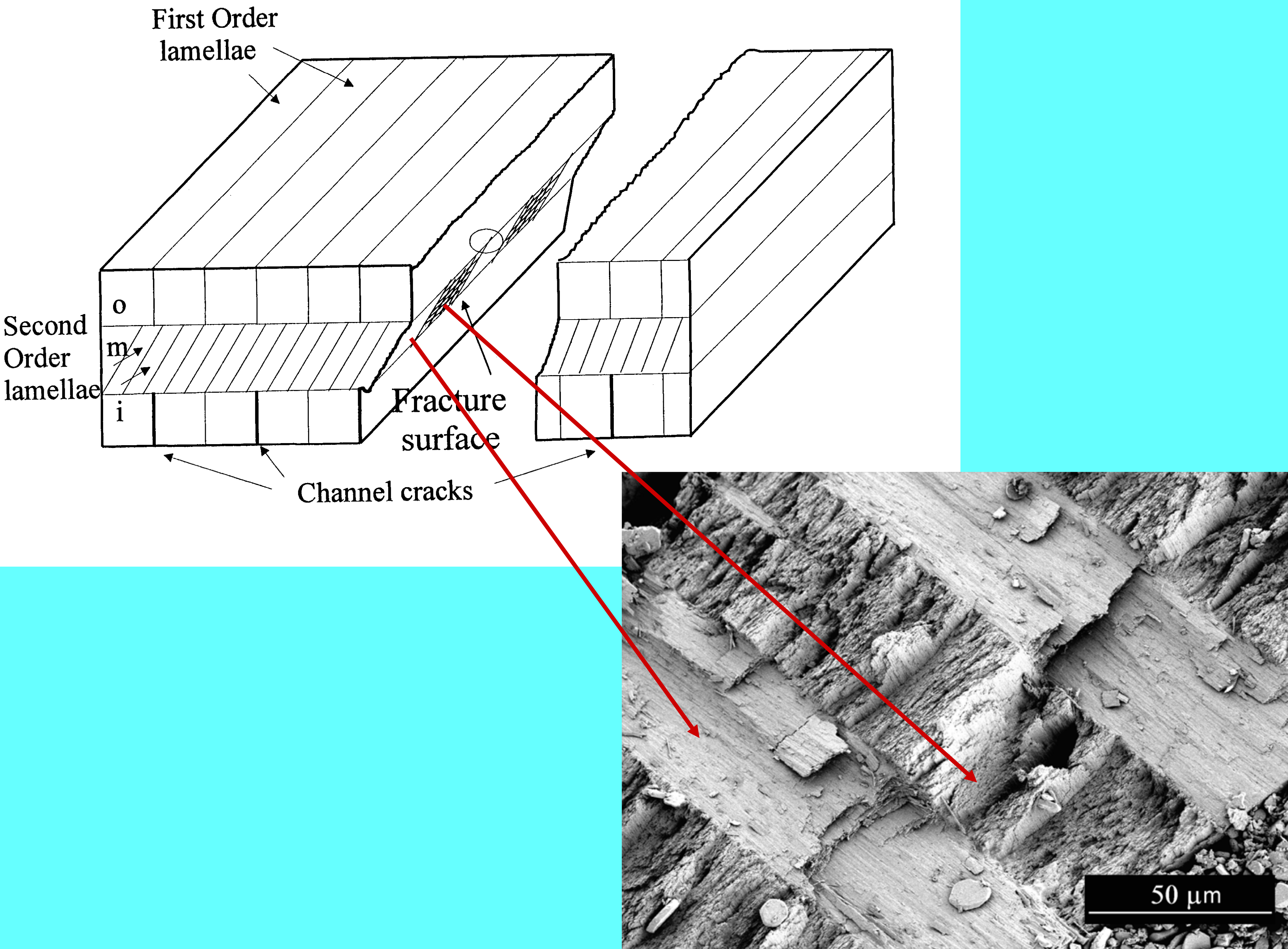
First Order
lamellae
Second
Order
lamellae
o
m
i
Fracture
surface
Channel cracks
50 μm

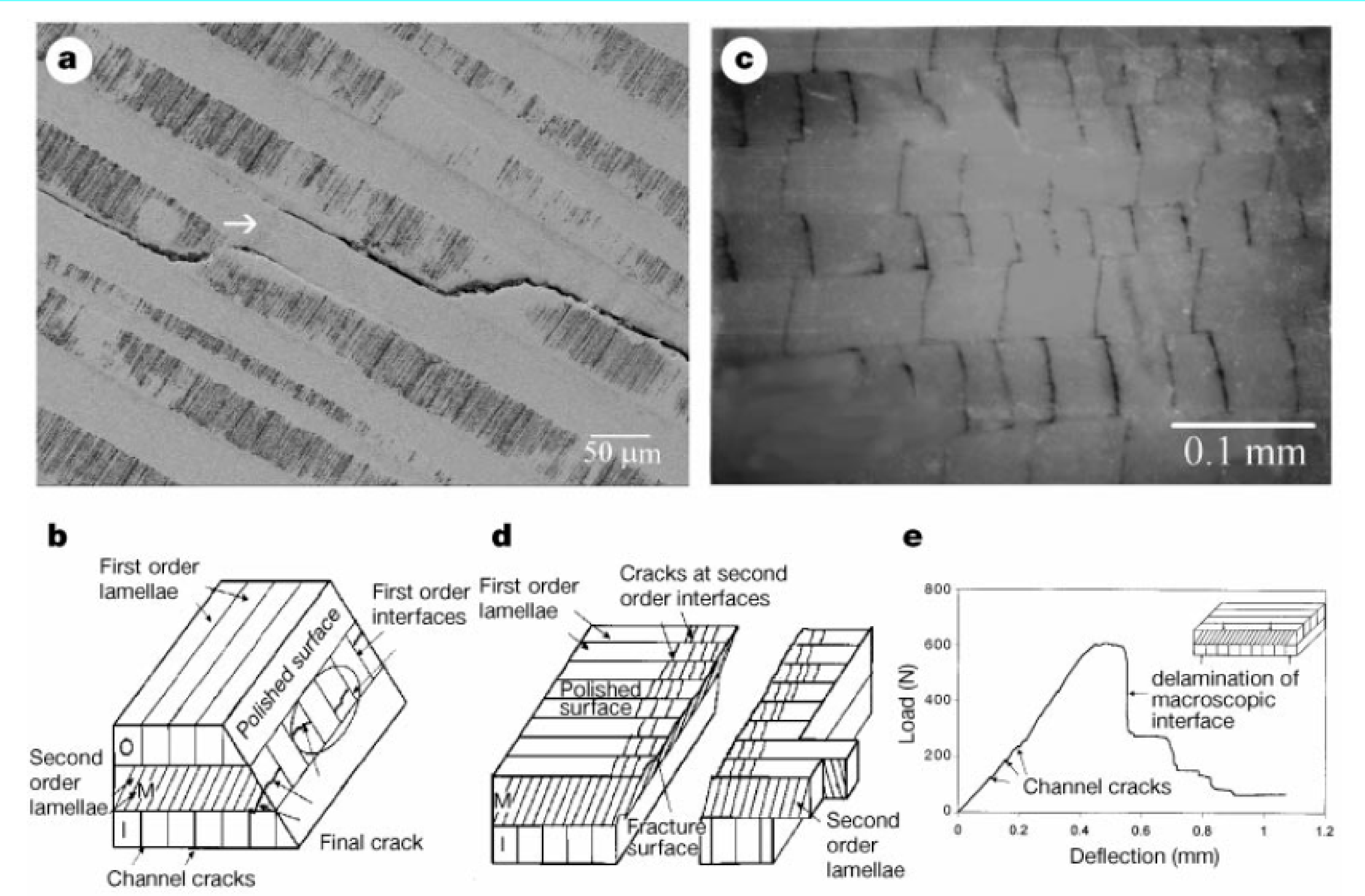
a
50 µm
c
0.1 mm
b
First order lamellae
First order interfaces
Polished surface
O
Second order lamellae
M
I
Final crack
Channel cracks
d
First order lamellae
Cracks at second order interfaces
Polished surface
M
I
Fracture surface
Second order lamellae
e
Load (N)
Deflection (mm)
delamination of macroscopic interface
Channel cracks
0
200
400
600
800
0
0.2
0.4
0.6
0.8
1
1.2

Multiple cracking of weak interfaces

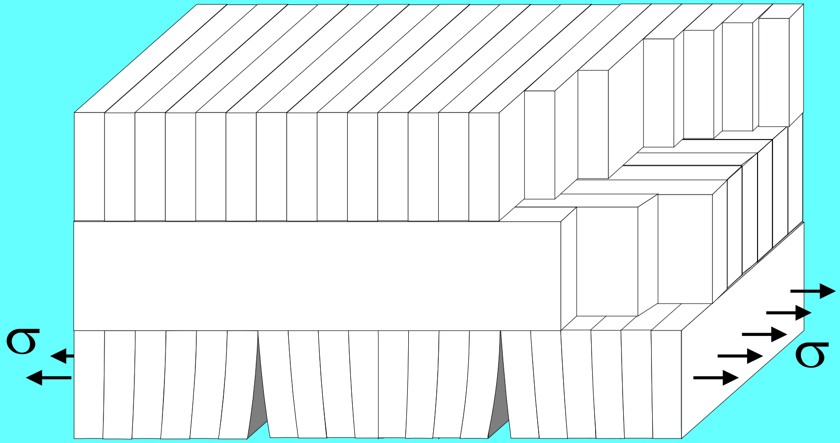

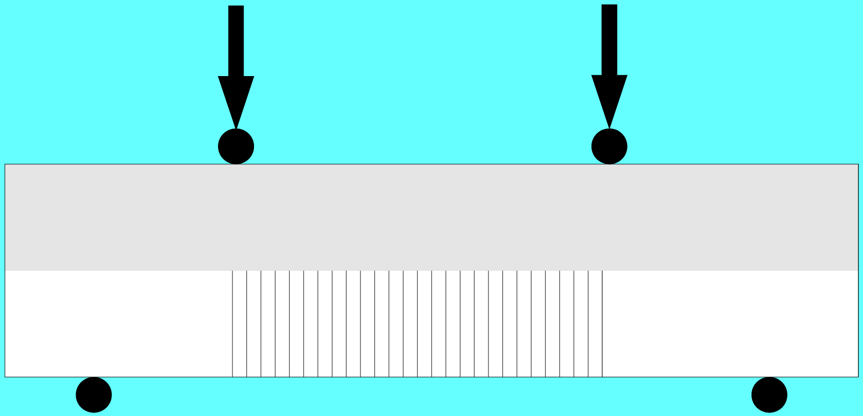

Basic idea (toughening)

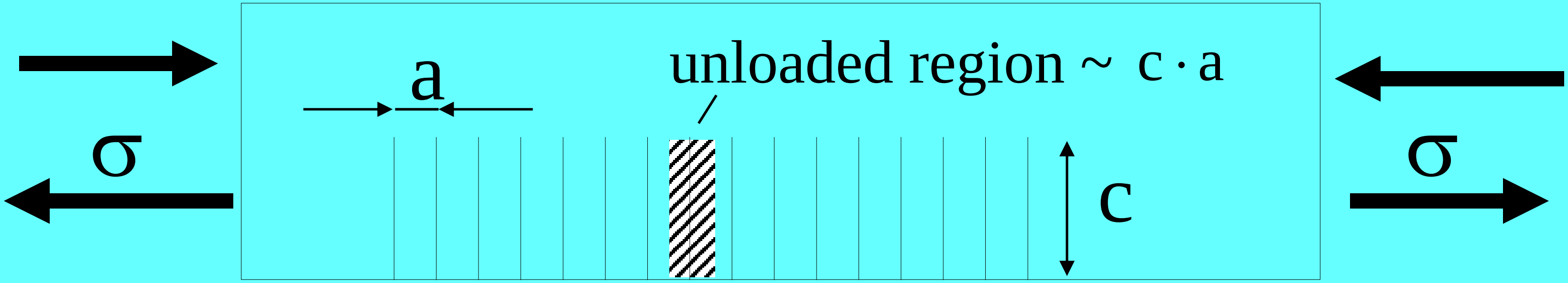

<u>Crack energy balance</u> :

strain energy $\longrightarrow$ $c \cdot a \times \dfrac{\sigma^2}{E} \sim c \times \gamma$ $\longleftarrow$ surface energy

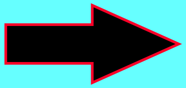 Critical stress $\boxed{\sigma_c \sim \left(\dfrac{\gamma E}{a}\right)^{1/2} \sim \dfrac{K_c}{a^{1/2}} >> \dfrac{K_c}{c^{1/2}}}$

Cracking conditions

steady state growth
from large flaws

$$\left(\frac{\partial U_{total}}{\partial n}\right)_{\varepsilon} = 0$$

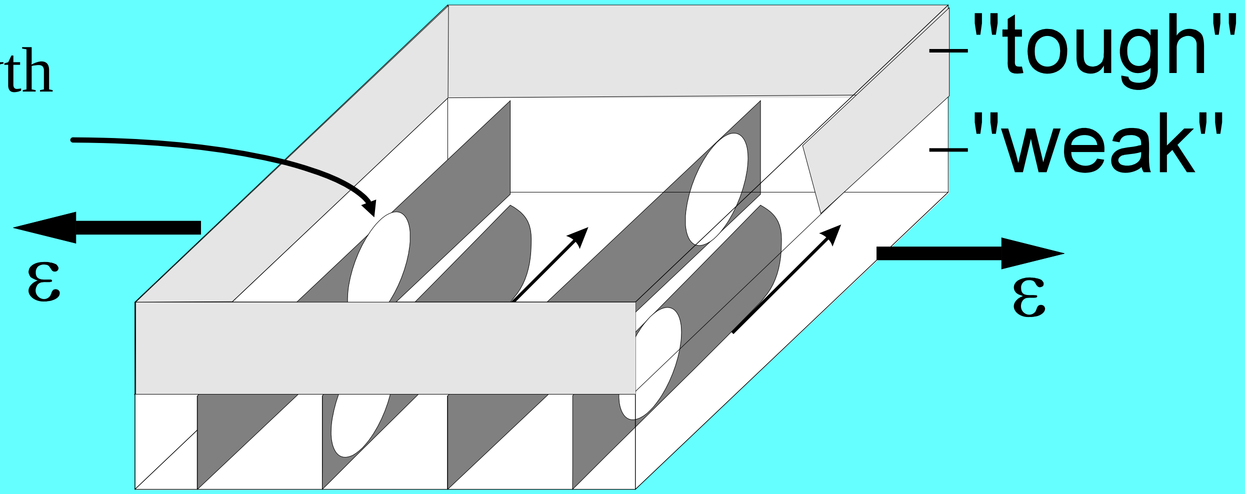

initiation of small flaws
by critical surface stress

$$\sigma_{surface}(\varepsilon) = \sigma_c$$

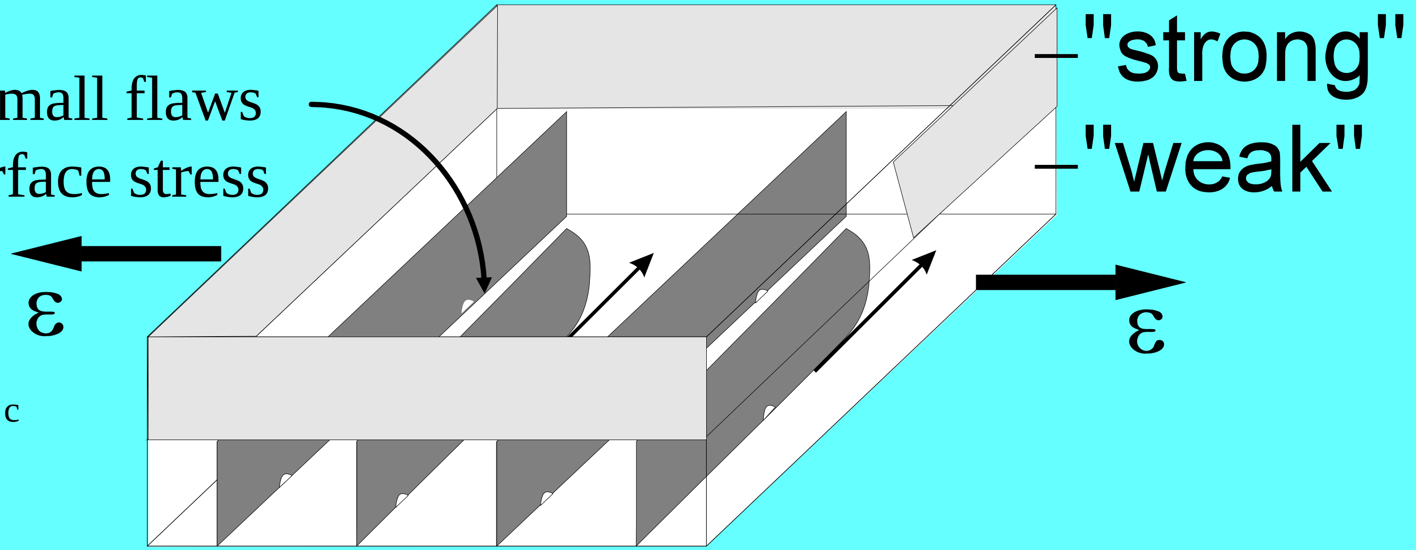

System of basic equations

Crack density evolution in the weak layer

large flaws $\quad U_{surface}(n) + U_{strain}(n, \varepsilon) = \mathrm{Min}(n)$

small flaws $\quad \sigma_{surface}(\varepsilon, n) = \sigma_c = \mathrm{const}$

$\left.\begin{matrix} \\ \\ \end{matrix}\right\} \quad \begin{matrix} n = n(\varepsilon) \\ \sigma = \sigma(\varepsilon) \end{matrix}$

Failure criterion of the strong layer

$K_I(\varepsilon) = K_{c1} \longrightarrow$ strain to failure, stress to failure and work of fracture

The model

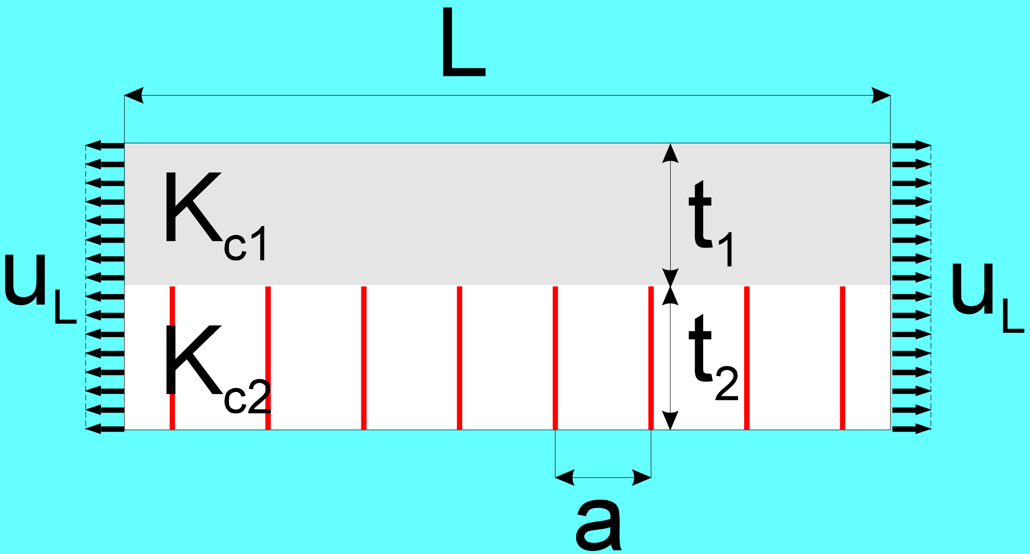

crack density

$n = (t_1 + t_2) / a$

$c = t_2 / (t_1 + t_2) = 1/2$

crack length

- bending $\longrightarrow$ tension
- 2 uniform layers with fracture toughness $K_{c1} > K_{c2}$
- failure at $K_I = K_{c1} = (2\gamma_1 E / (1-\nu^2))^{1/2}$
- plane strain

Shape function determination

$$f(n) = \frac{1}{2}\left(1 + \frac{1}{1 + 2\cdot\left|f'(0)\right|\cdot n}\right)$$

$$k(n) = \left(\frac{1 + pn}{1 + qn + sn^2}\right)^{1/2}$$

$$g(n) = \frac{1 - n/n_o}{1 + 8n - 5n^{3/2} + n^6}$$

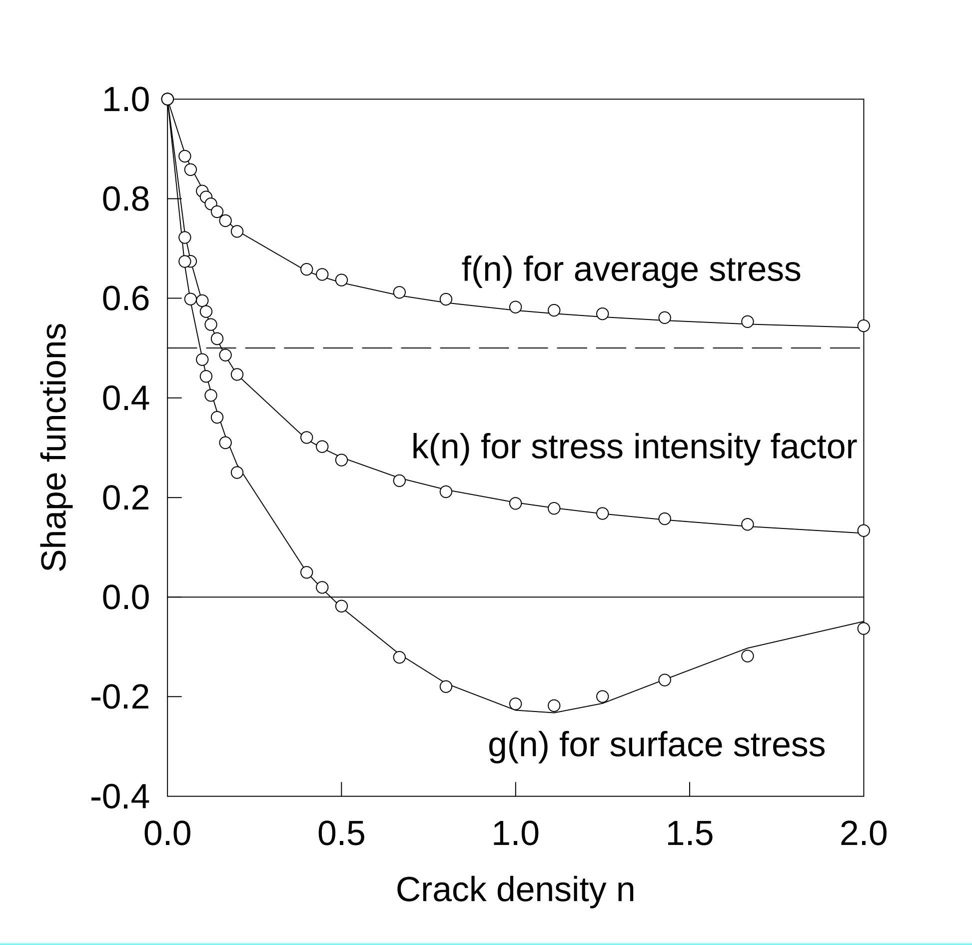

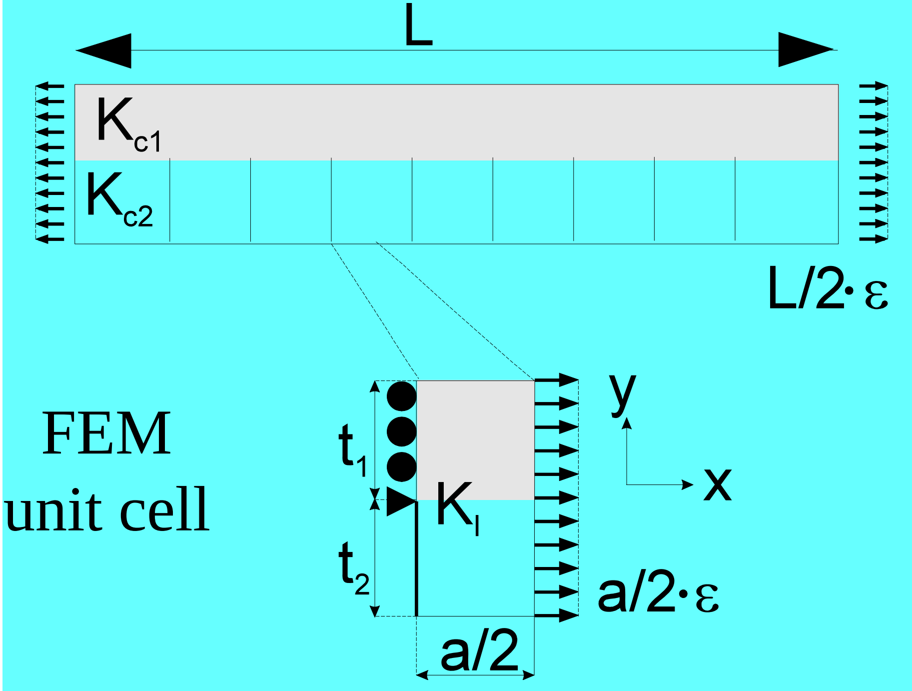

Analysis

- ? crack density evolution $n=n(\varepsilon)$
- ? stress-strain curve $\sigma=\sigma(\varepsilon)$
- ? failure stress and strain $\sigma_{failure}$, $\varepsilon_{failure}$
- ? work of fracture $W_{fracture}$

Crack density at failure

Large flaws

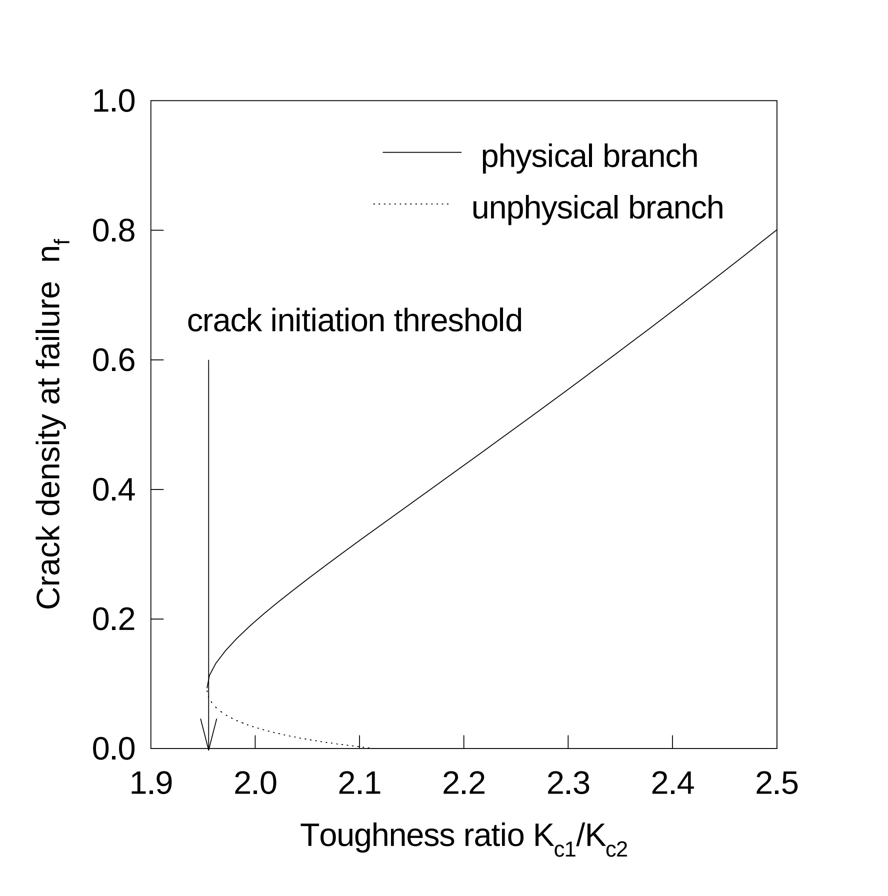

Small flaws

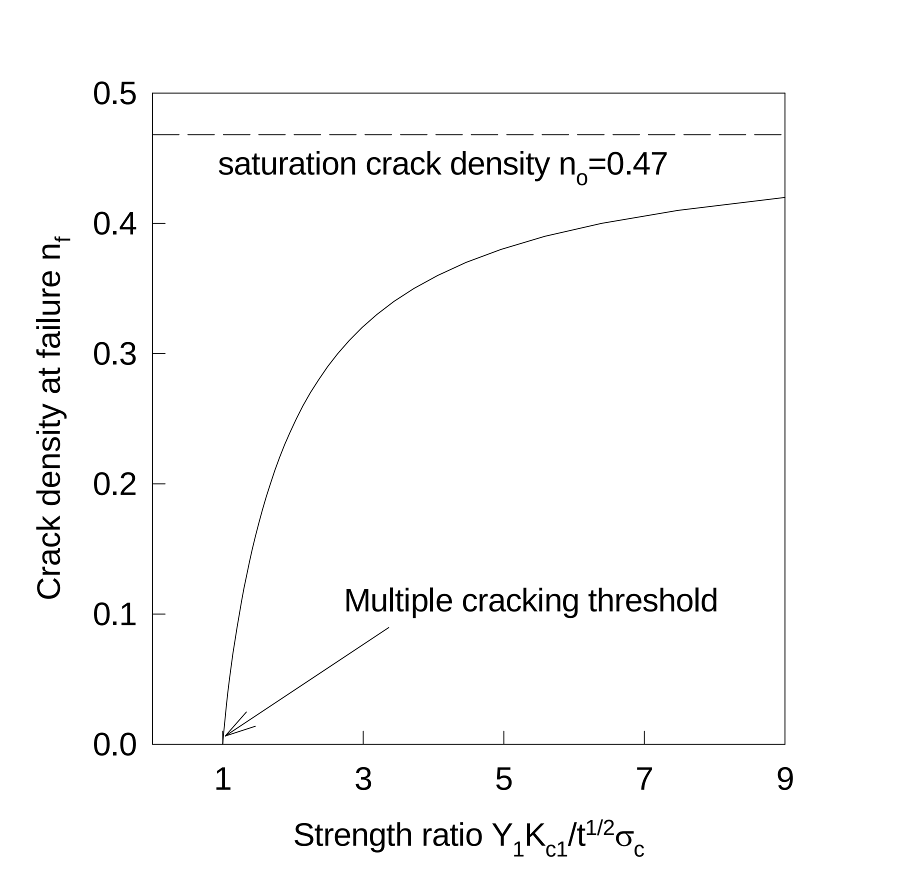

Stress and strain to failure

Large flaws

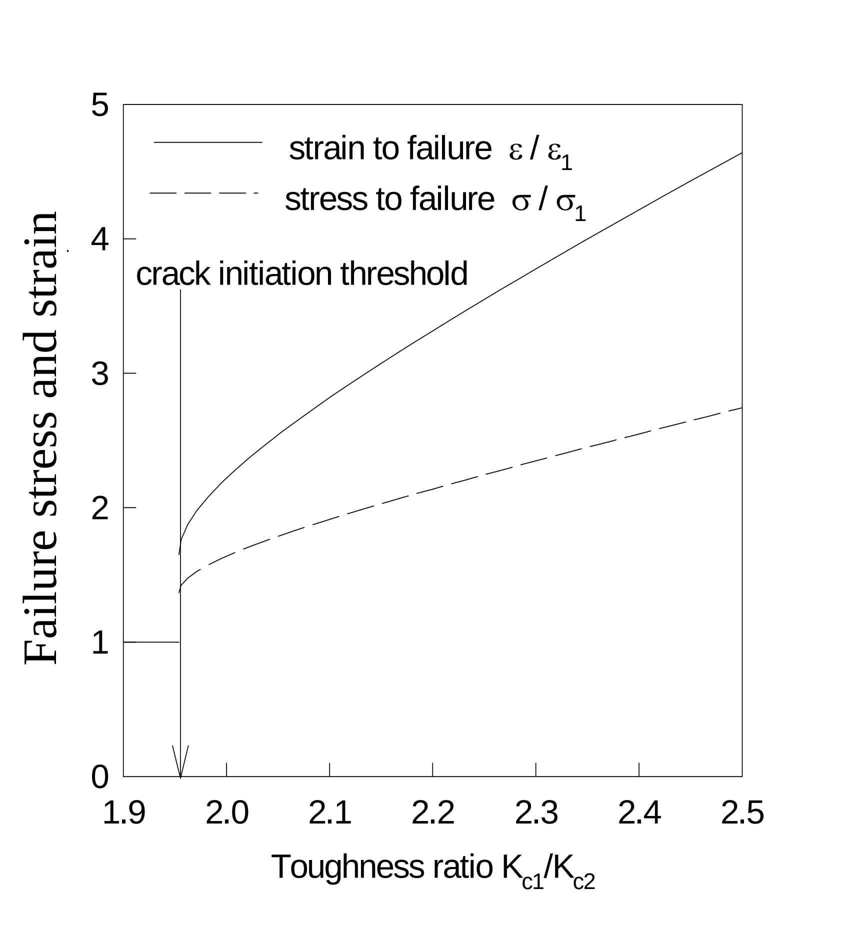

Small flaws

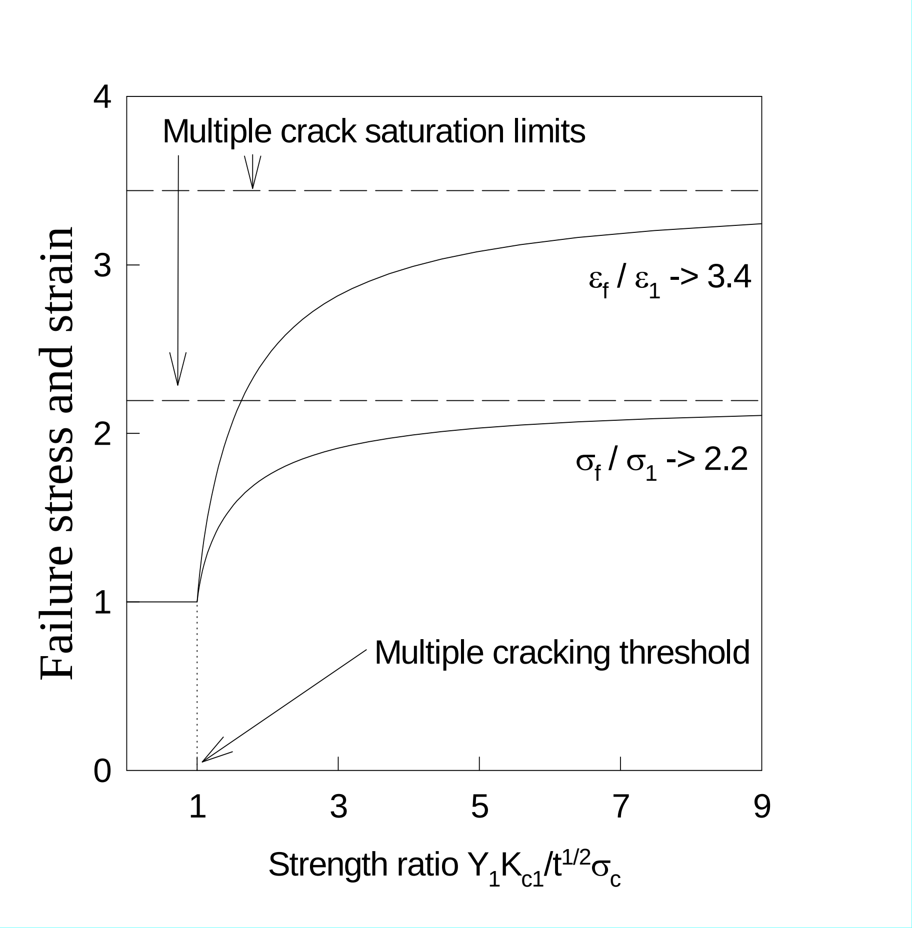

Work of fracture

Large flaws

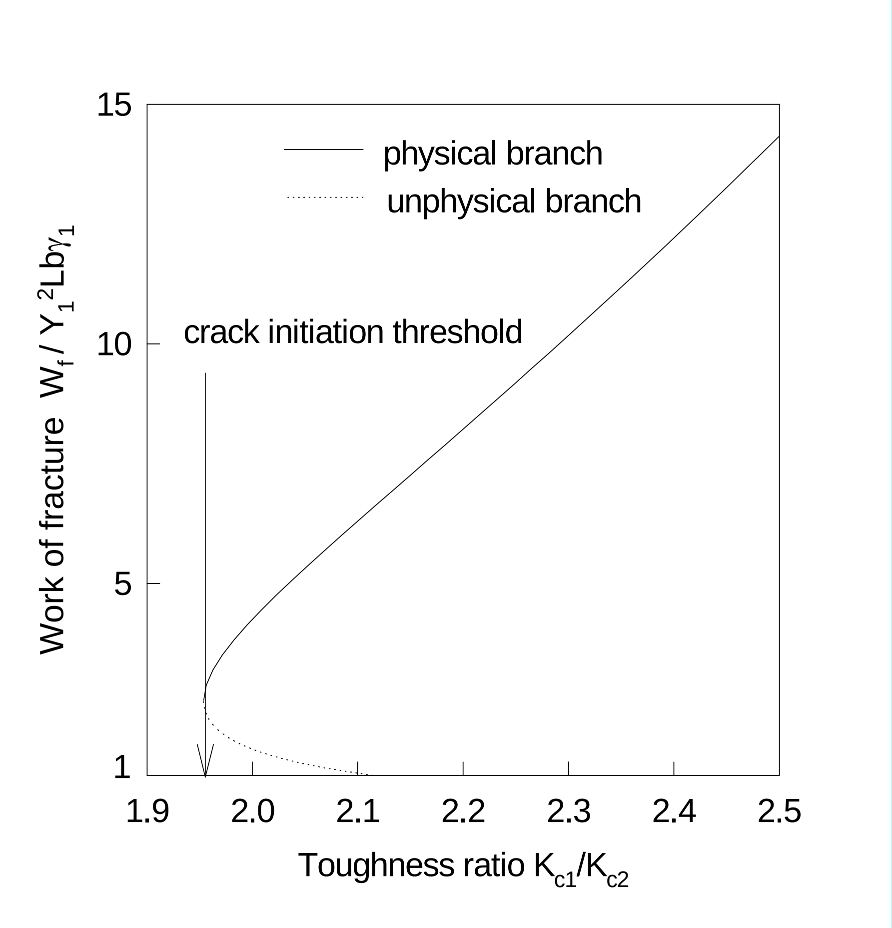

Small flaws

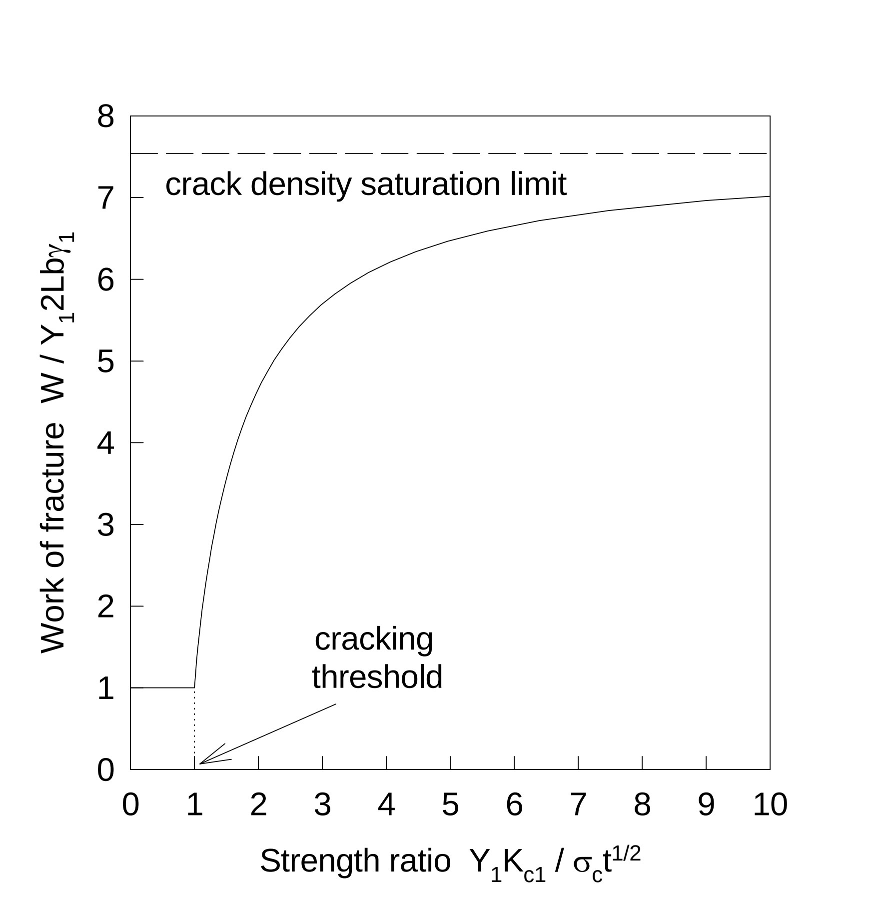

LARGE SCALE BRIDGING

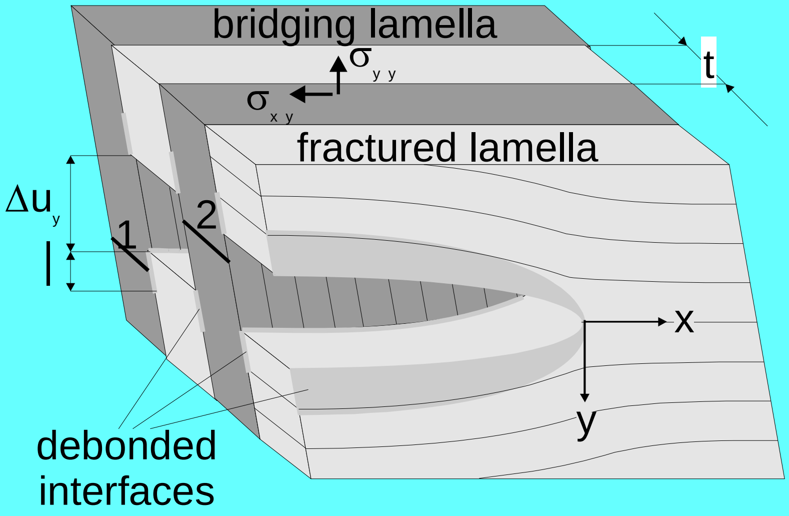

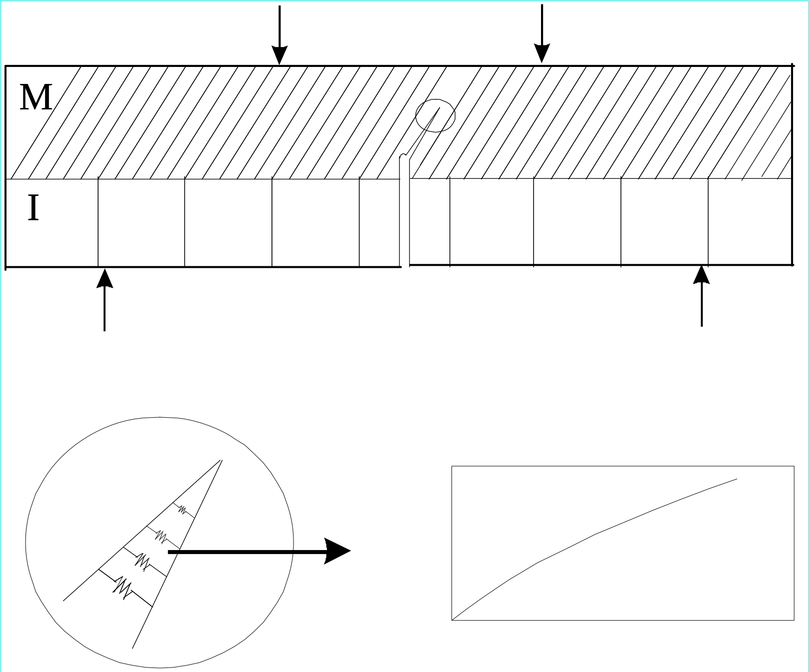

$$K_{protein} = K_{far\text{-}field} - K_{bridging\ forces} = 0.6 MPa\text{-}m^{1/2}$$

$$p = \beta * u^{1/2} : \ \beta = 630\ N/mm^{5/2},\ u_{crit} = 5\ \mu m$$

$$J_b = \int_0^{u_{cr}} p(u)du = 150 N/m$$

$$J_{aragonite} = (K^2/E)_{aragonite} = 0.63 N/m$$

$$J_{int} = 0.6^2/37 GPa = 9.7 N/m$$

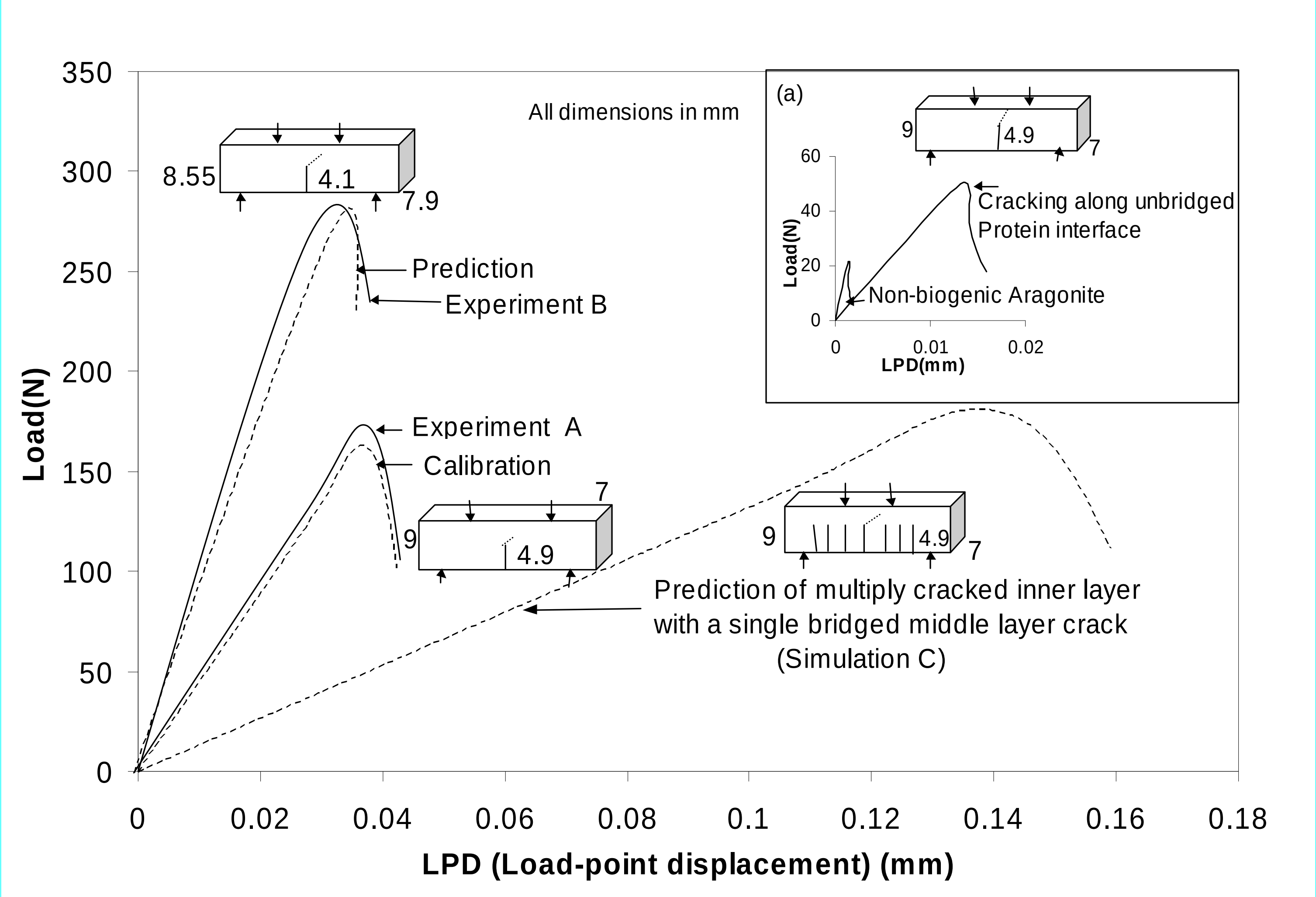

WORK OF FRACTURE (E-3J)

Aragonite	Protein	Notched A	Multiply Cracked
0.07	0.4	5.8	23

-120ºC

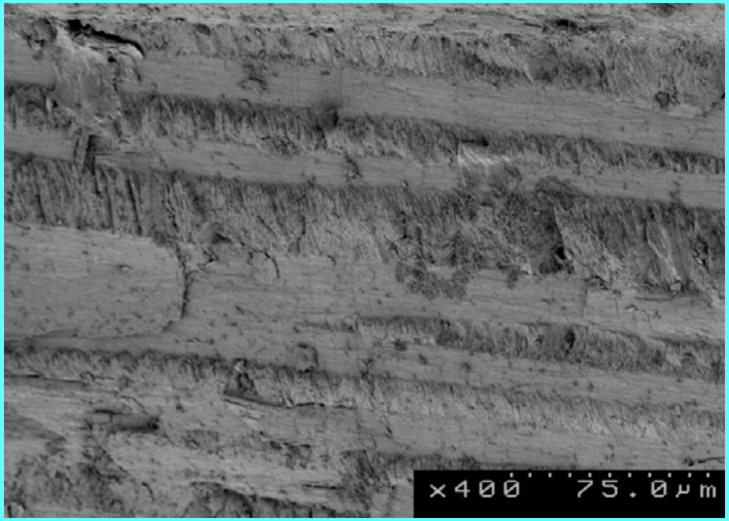

200ºC

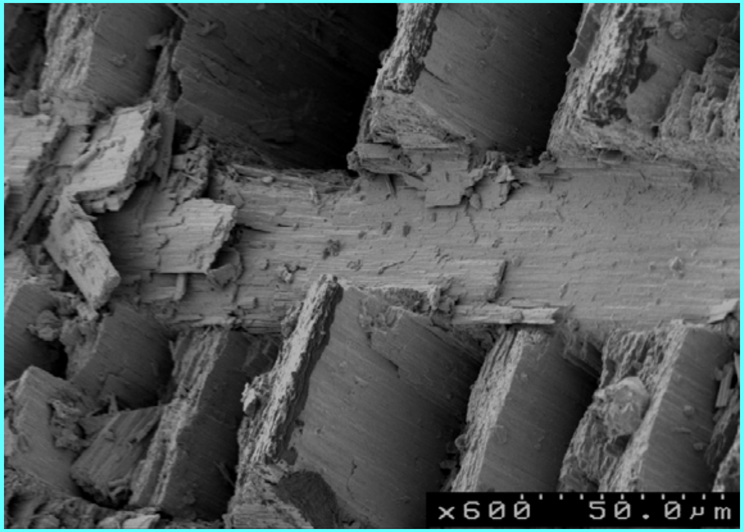

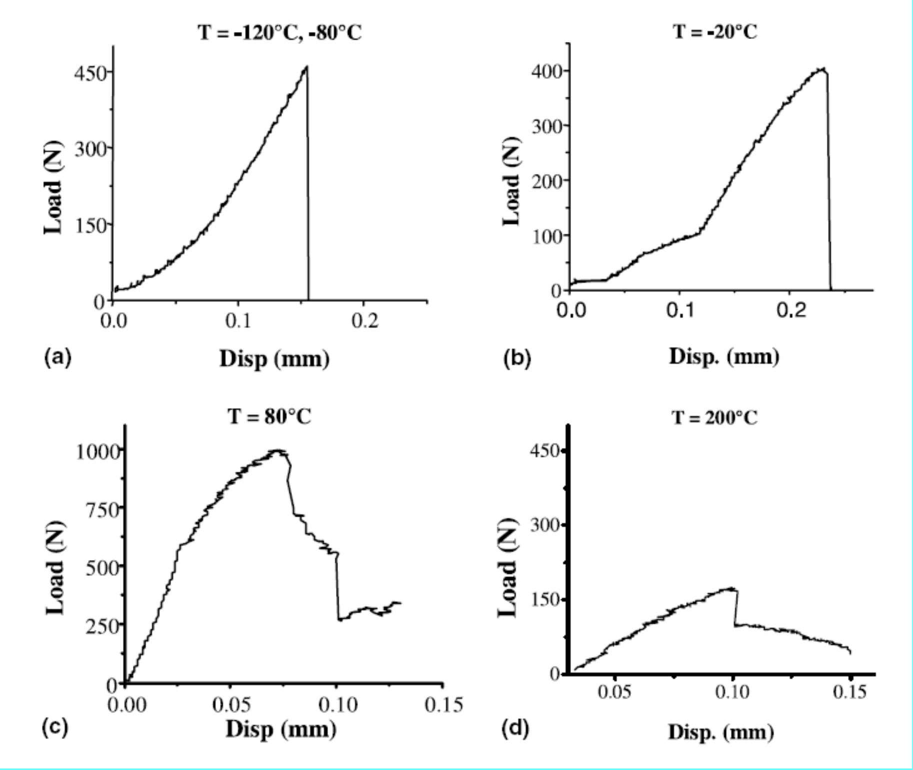

Role of the binder

Modular Elongation Mechanism

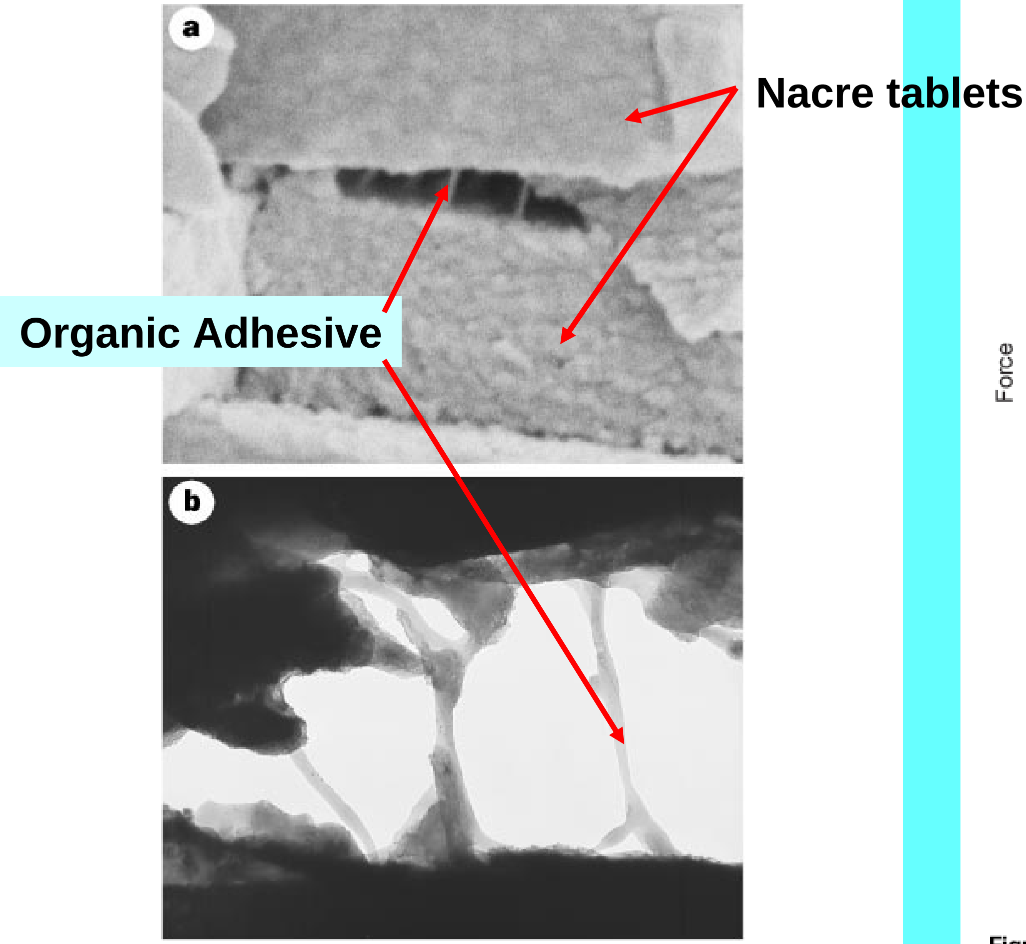

Figure 1 Scanning and transmission electron micrographs of a freshly cleaved abalone shell, showing adhesive ligaments formed between nacre tablets. **a**, Scanning electron micrograph of a freshly cleaved abalone shell showing adhesive ligaments formed between consecutive abalone nacre tablets on exertion of mechanical stress. The tablets are ~400 nm thick. **b**, Transmission electron micrograph of another cleaved abalone shell, showing the adhesive ligaments between nacre tablets. The space between the tablets is ~600 nm. Thus the ligaments can lengthen to many times the original spacing between the tablets, which is of the order of 30 nm.

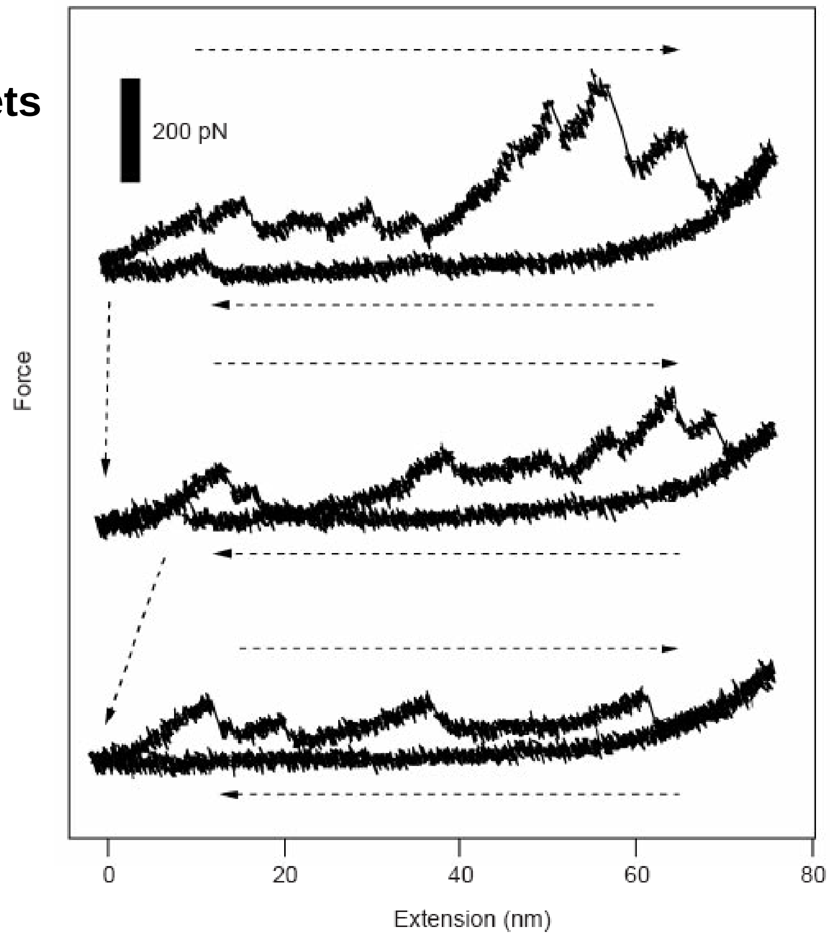

Figure 2 Consecutive force–extension curves, obtained using an atomic force microscope, from pulling on a freshly cleaved abalone nacre surface. Rupture events, with a sawtooth appearance, are visible in each of the curves. The surface was not touched between pulls, strong evidence that some refolding took place, possibly of domains in lustrin A. The approach and retract curves show hysteresis, indicating that the rupture events dissipate energy.

B.L. Smith et al., Nature, 1999

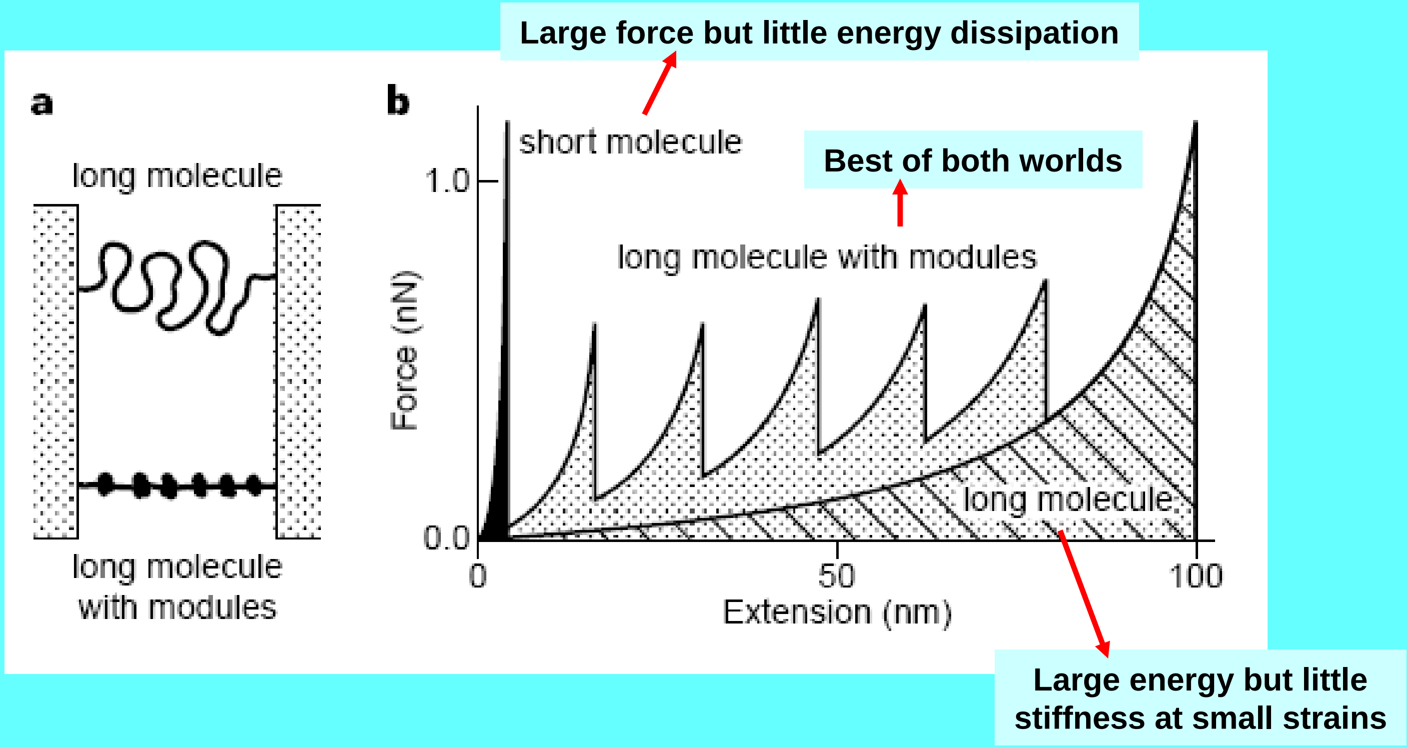

Large force but little energy dissipation
a
long molecule
long molecule
with modules
b
short molecule
Best of both worlds
long molecule with modules
long molecule
1.0
0.0
Force (nN)
0
50
100
Extension (nm)
Large energy but little
stiffness at small strains

AVESTON-COOPER-KELLY LIMIT
for fiber-bridged cracks

$$k\int_0^L \frac{b(t)dt}{t-x} \;+\; \sigma^{\infty} \;+\; \Im\left[\int_x^L b(t)dt\right] = 0 \;,\quad 0 < x < L$$

$$COD \sim \int_x^L b(t)dt$$

AVESTON-COOPER-KELLY LIMIT

Under uniform tension, all ligaments remain intact as crack propagates across specimen.

Specimen width is w~10mm

Initial notch is c_o~5mm

$$\frac{\sigma_{cr}^{ACK}}{p_{cr}} = \left(\frac{2J_c^{\text{int}}}{J_b}\right)^{1/3} \sim 0.5 \longrightarrow$$

Noncatastrophic failure

$$a_m = \frac{\pi E'}{4}\left(\frac{3J_c^{\text{int}}}{2}\right)^{1/3} \beta^{-4/3} \sim 1mm \sim 0.1w \longrightarrow$$

Amount of crack growth required to achieve ACK limit; bridging effects increase with increasing w/a_m

$$a_m < c_o \longrightarrow$$

Growth from the notch is stable

$$a_s = \frac{2}{\pi}\left(\frac{p_o}{\sigma_{cr}}\right)^4 a_m \sim 20mm >> a_m \longrightarrow$$

Small scale bridging length scale; ACK limit would be reached in large enough specimen, and growth is stable in notched specimen

Schematic Drawing of Conch Shell

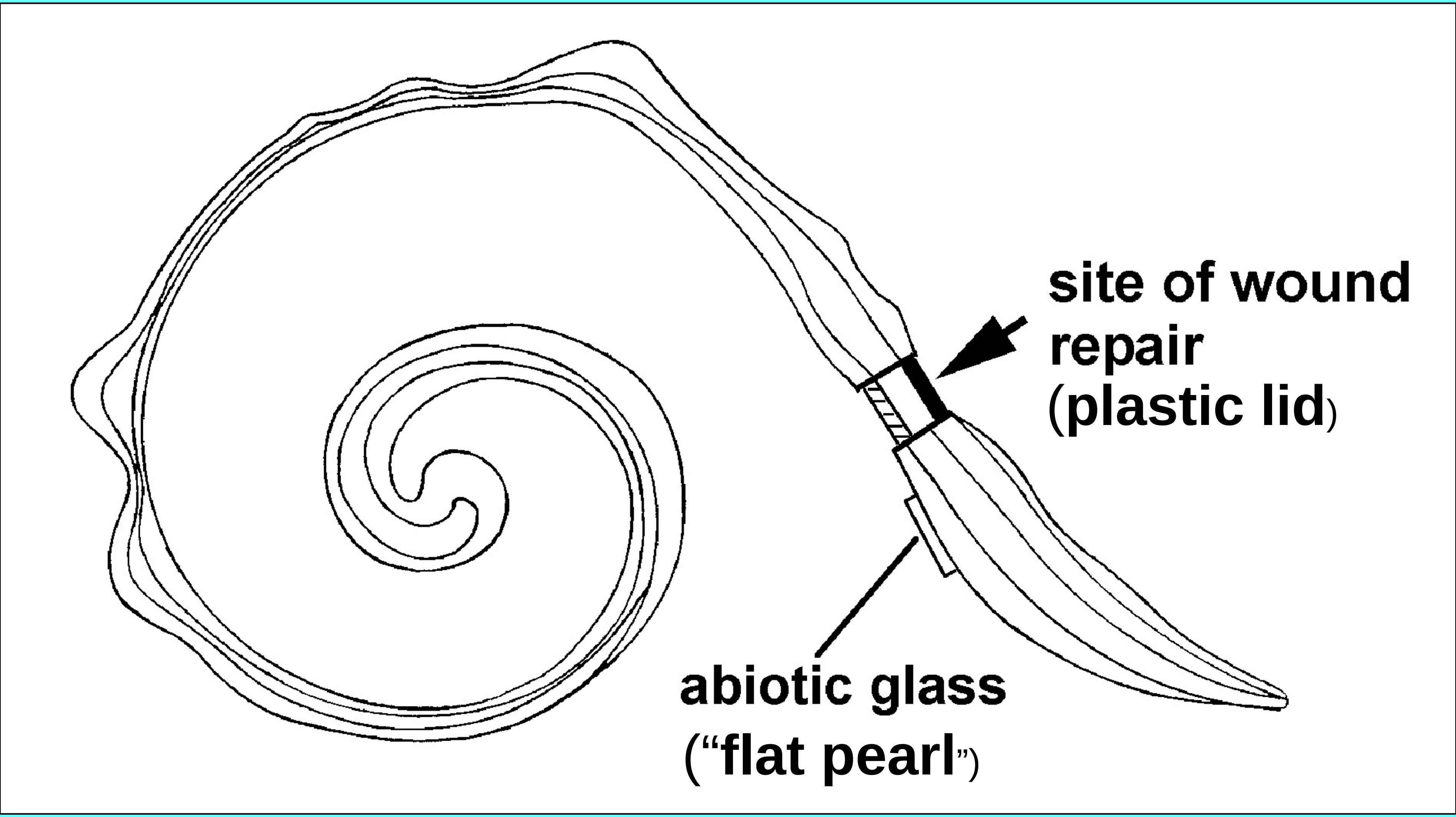

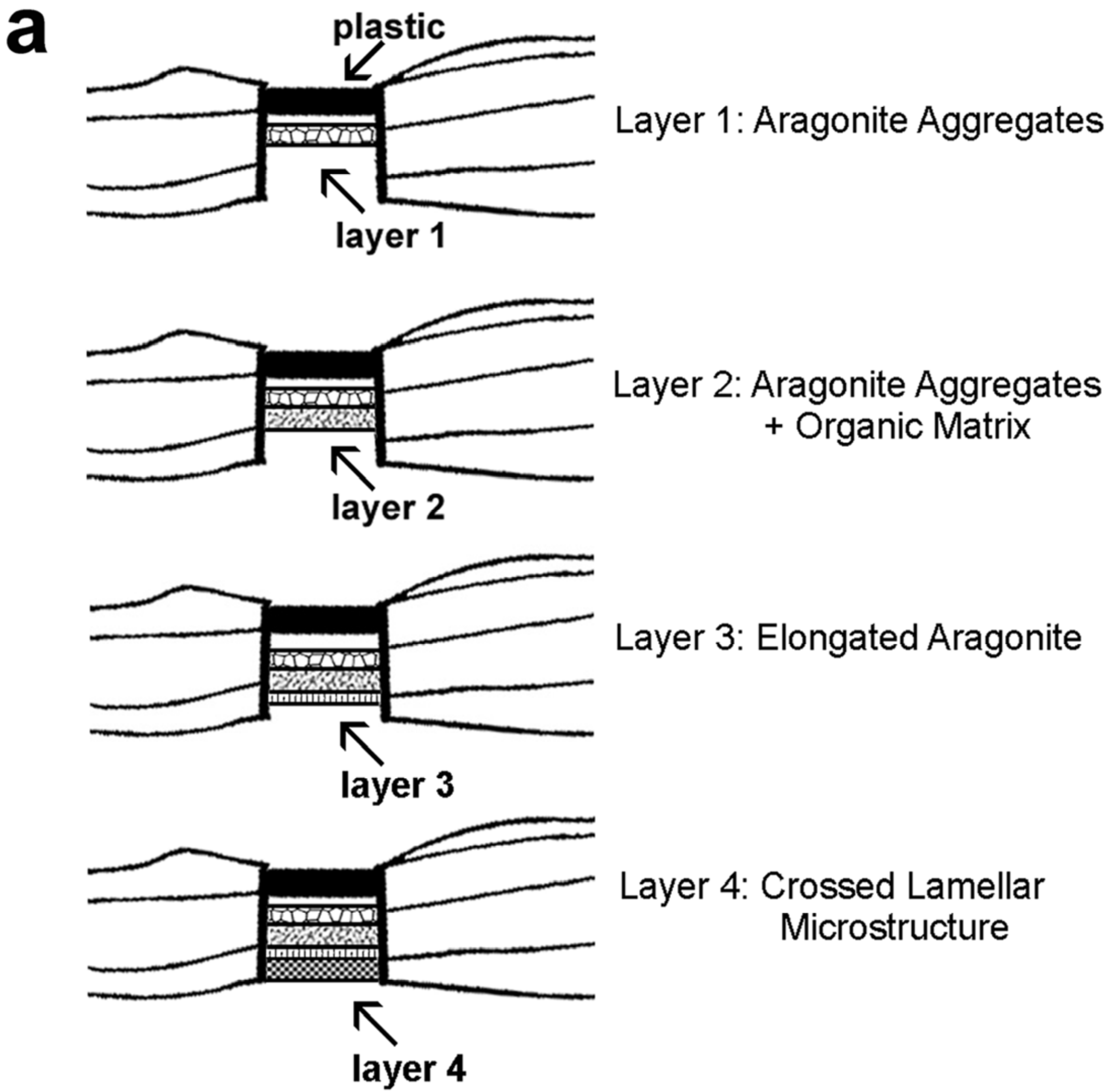
a
plastic
layer 1
Layer 1: Aragonite Aggregates
layer 2
Layer 2: Aragonite Aggregates
+ Organic Matrix
layer 3
Layer 3: Elongated Aragonite
layer 4
Layer 4: Crossed Lamellar
Microstructure

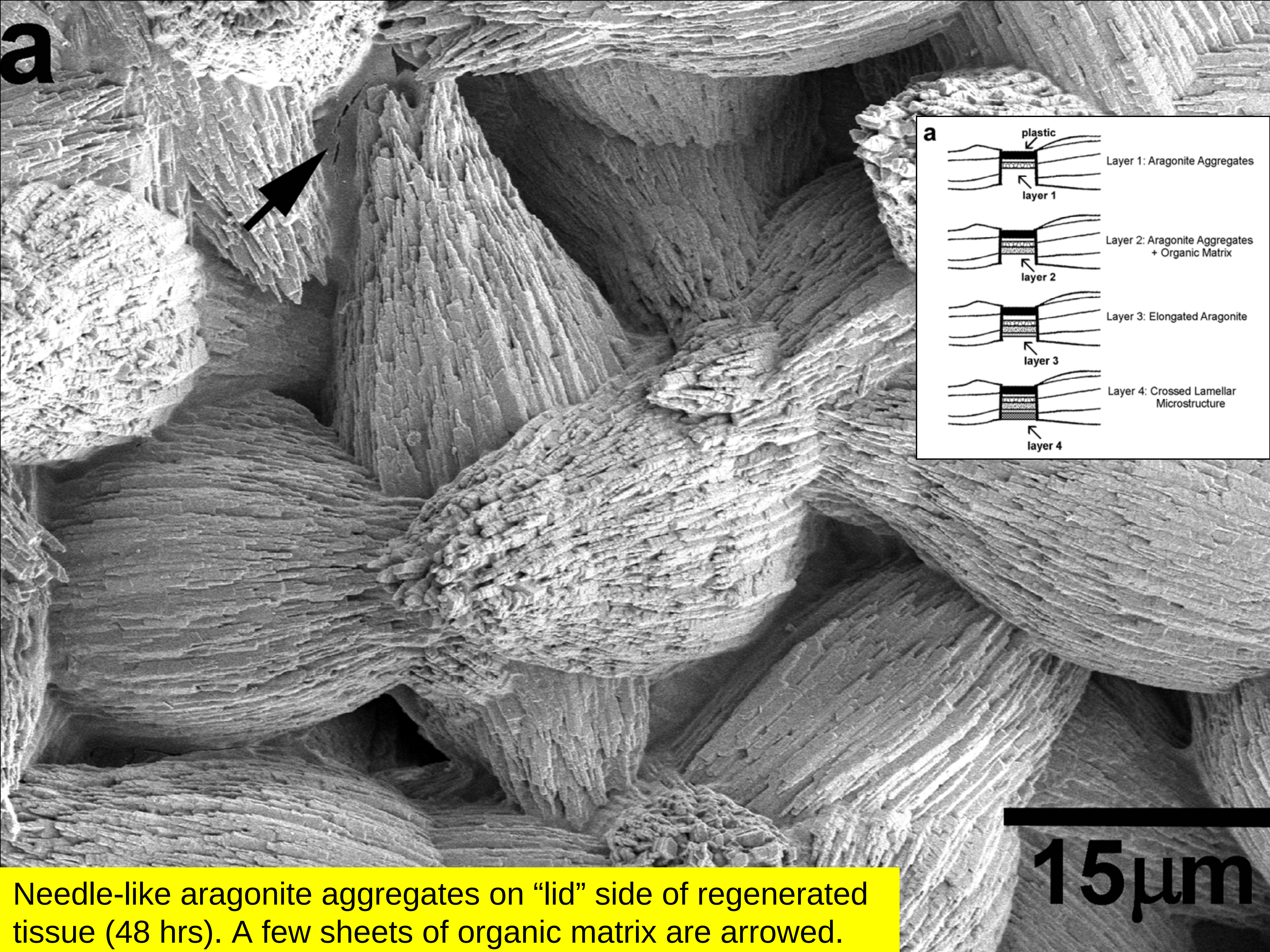

Needle-like aragonite aggregates on “lid” side of regenerated tissue (48 hrs). A few sheets of organic matrix are arrowed.

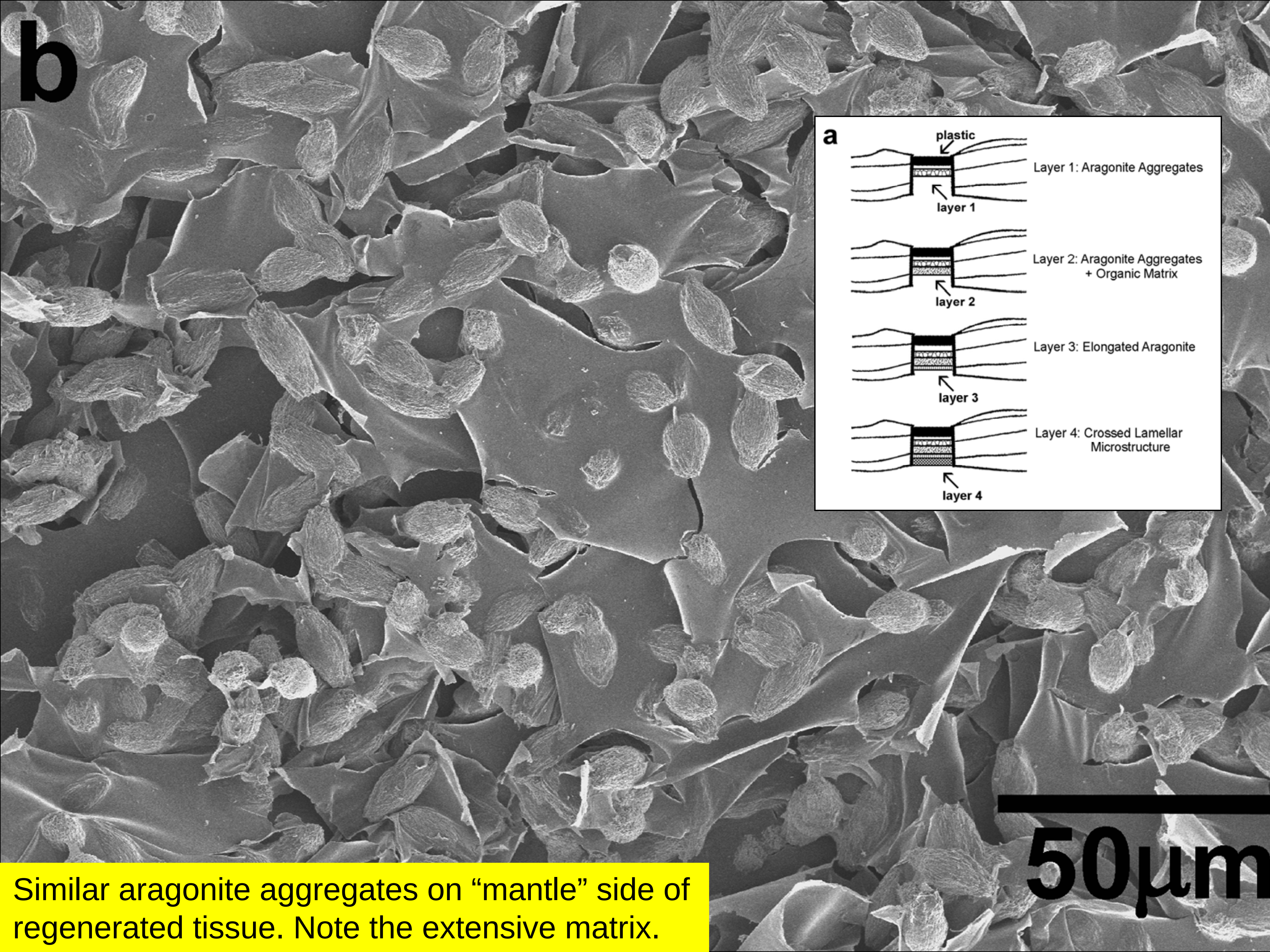

Similar aragonite aggregates on “mantle” side of regenerated tissue. Note the extensive matrix.

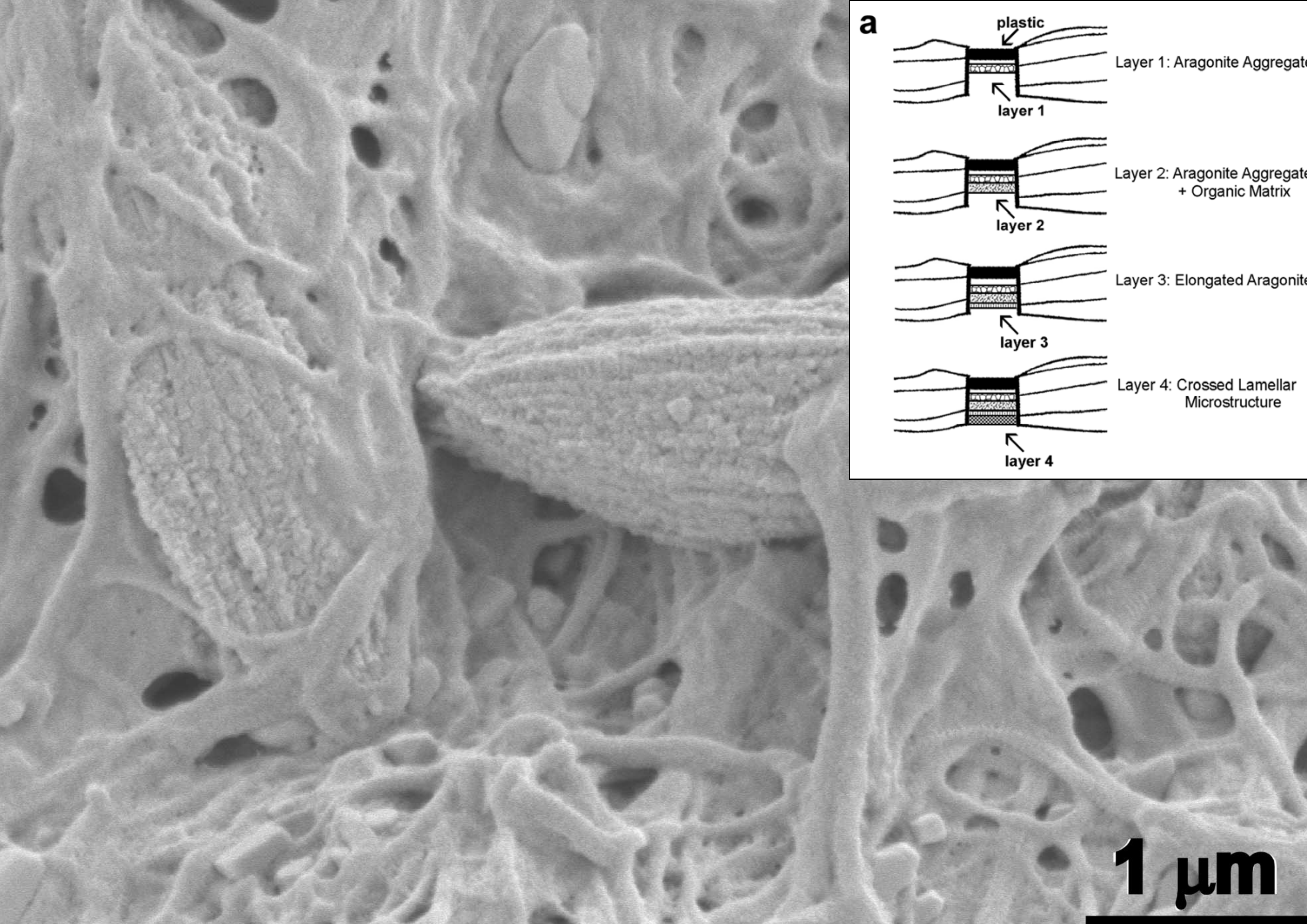

Aragonite aggregates within the collagenous matrix.

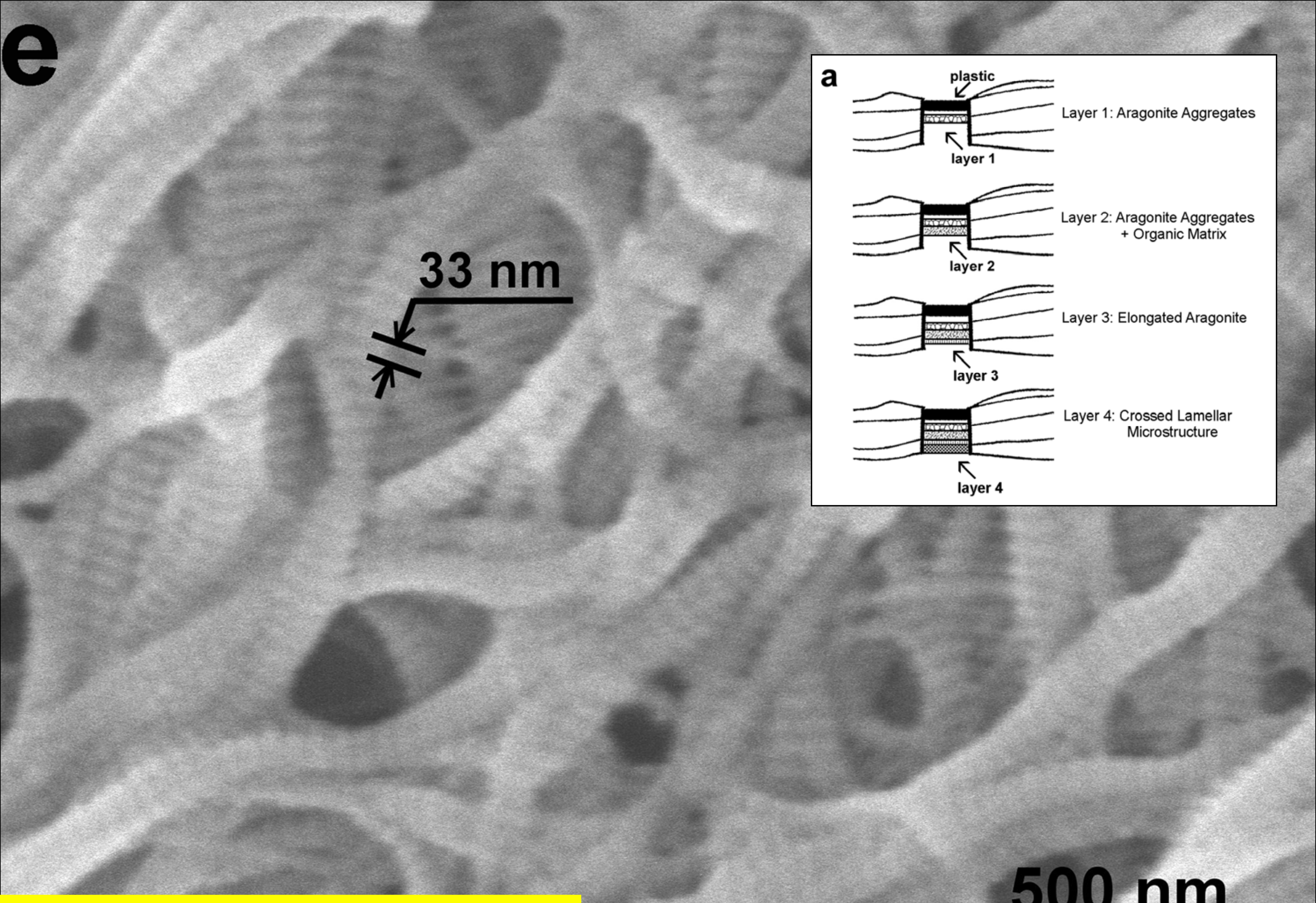

Collagenous matrix forms when wound repair occurs without the lid.

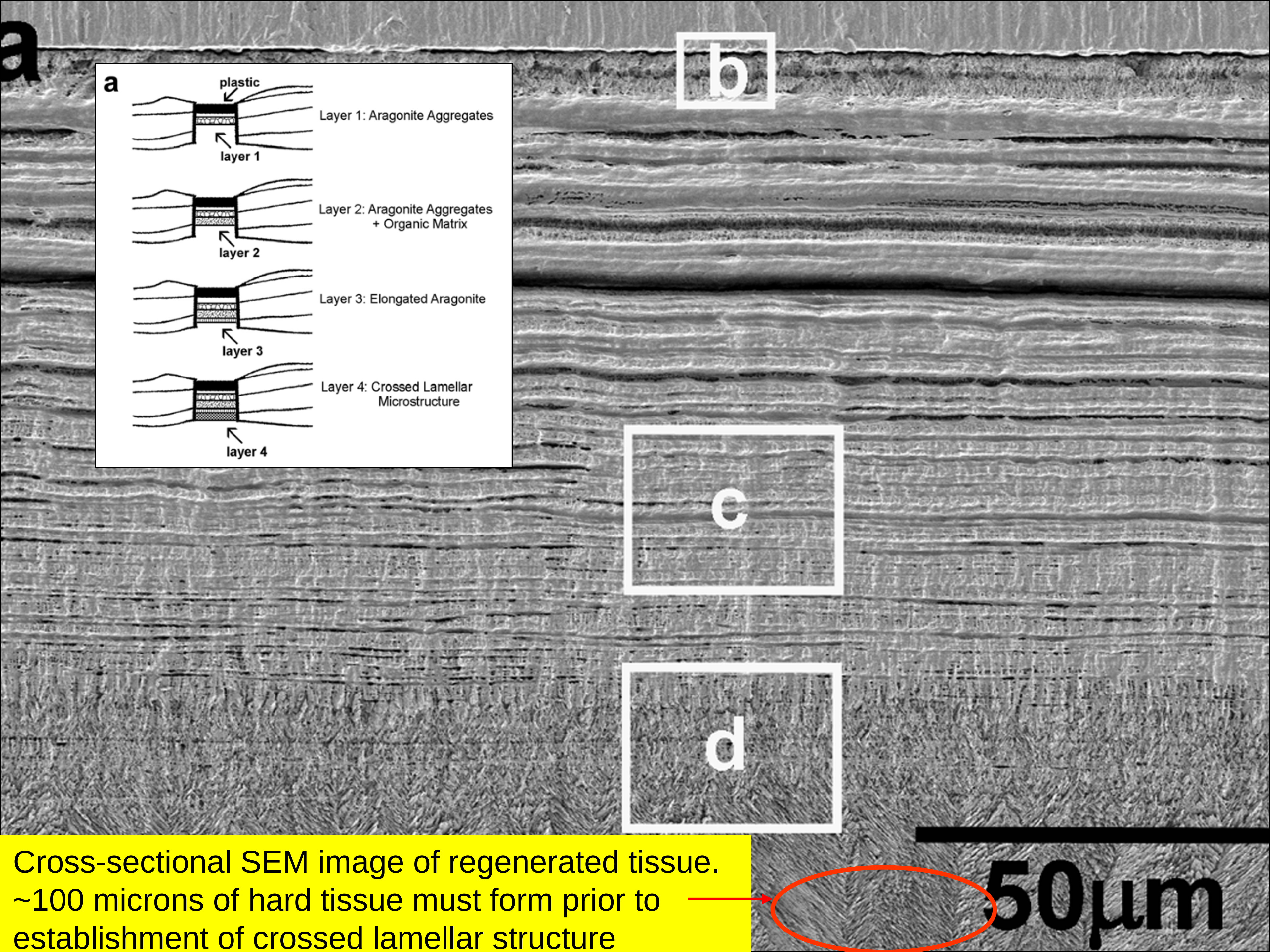

Cross-sectional SEM image of regenerated tissue.
~100 microns of hard tissue must form prior to establishment of crossed lamellar structure

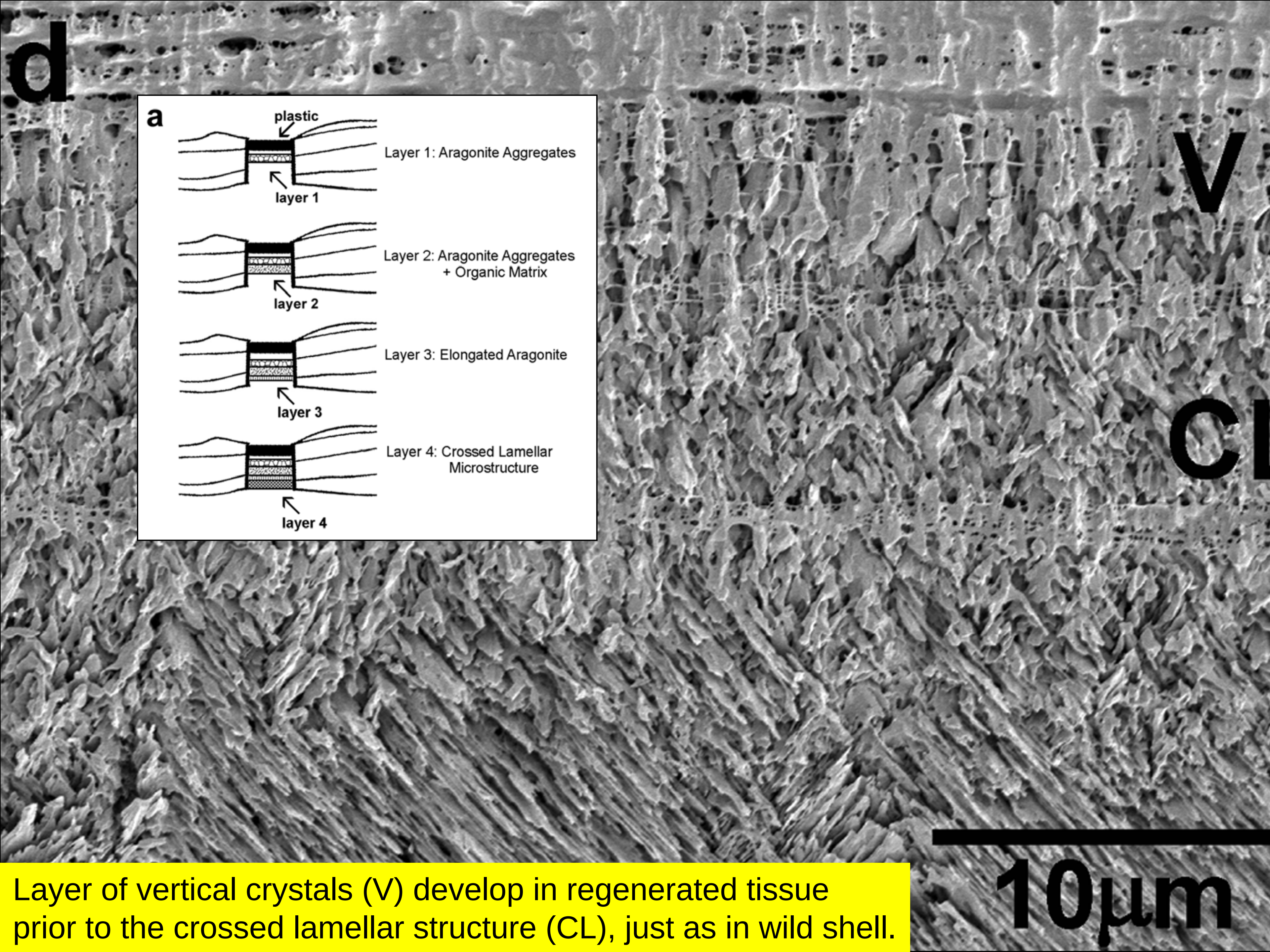

Layer of vertical crystals (V) develop in regenerated tissue prior to the crossed lamellar structure (CL), just as in wild shell.

BIOINSPIRED MEMS COMPOSITE STRUCTURES AS MODEL SYSTEMS

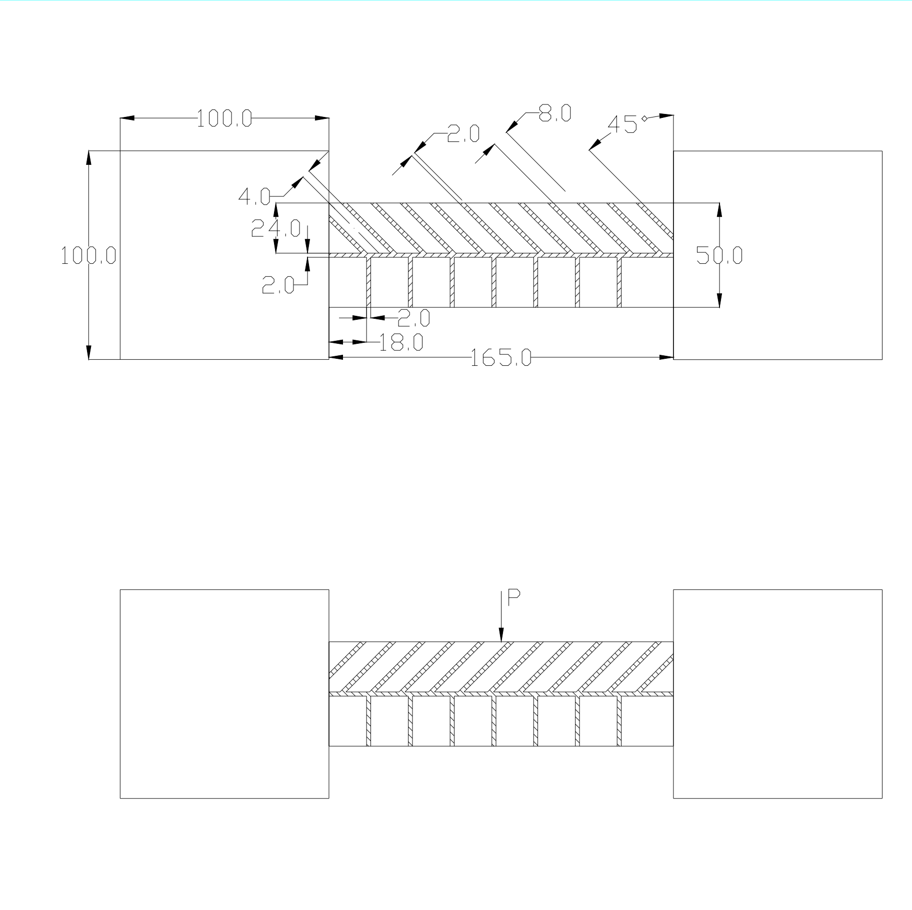

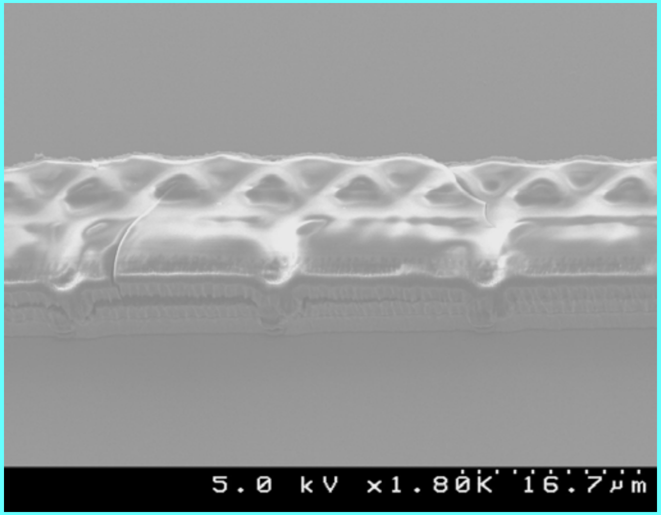

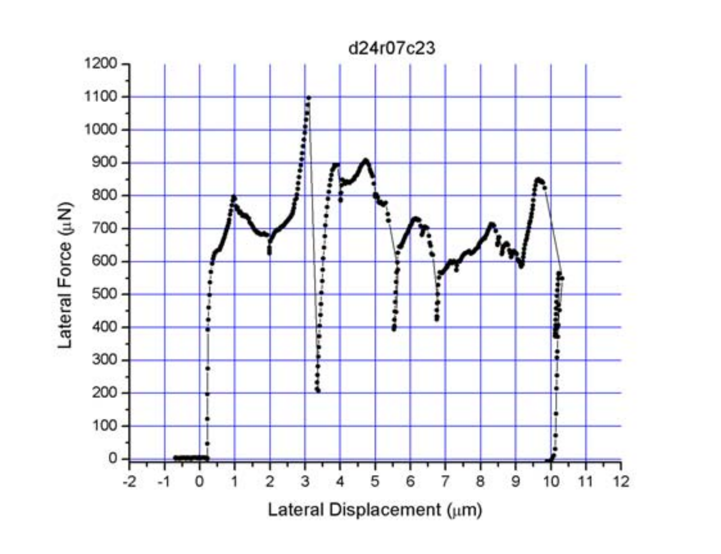

Bioinspired polysilicon/polymer MEMS Structures

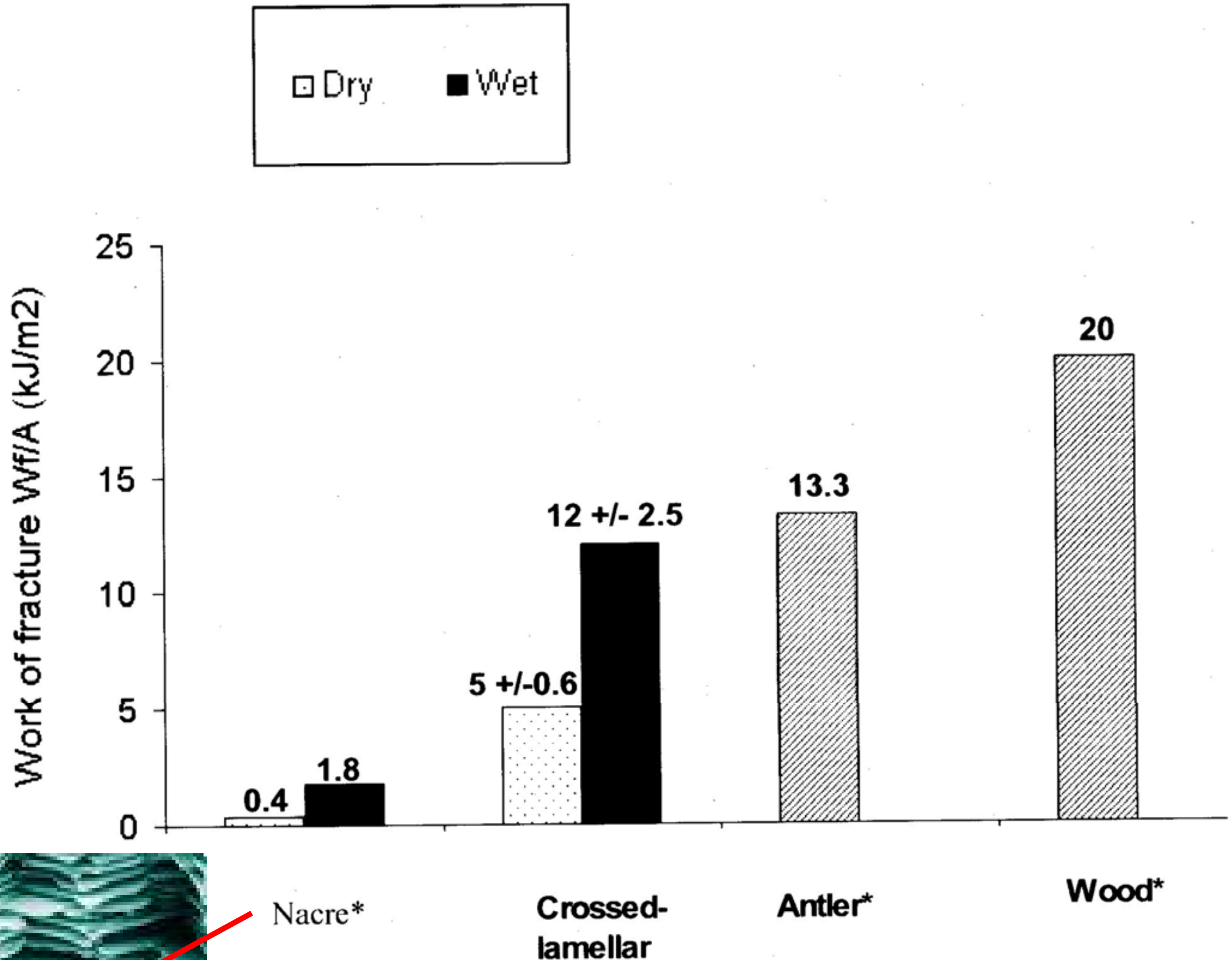

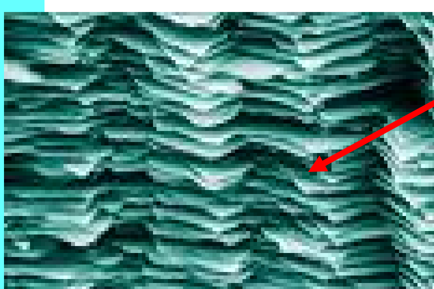

A.A.Jackson, J.F.V. Vincent and R.M. Turner (1990)
J. Mat. Sci. 25, p3137

Bioinspired Fabrication of Composites: Synthetic Nacre

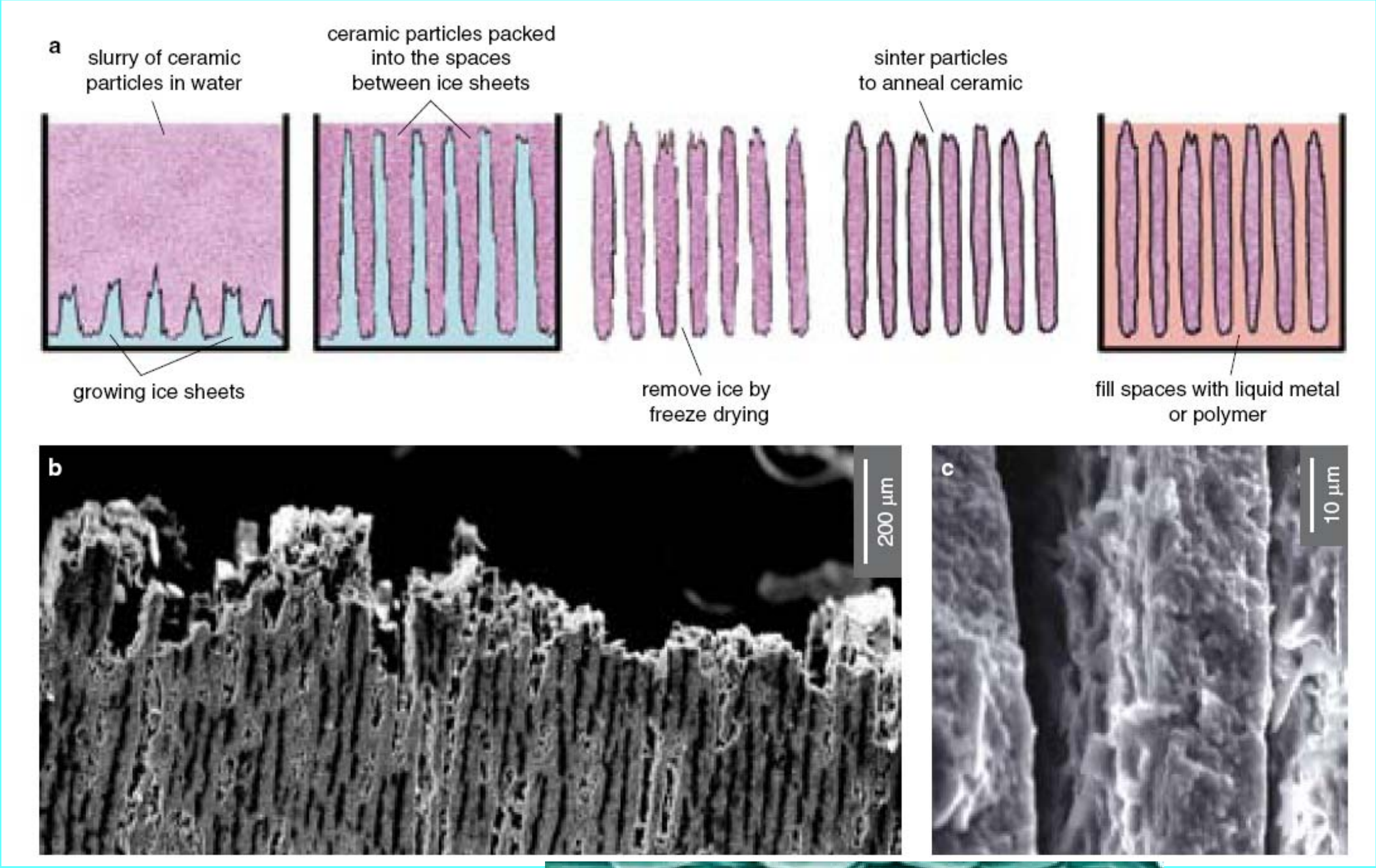

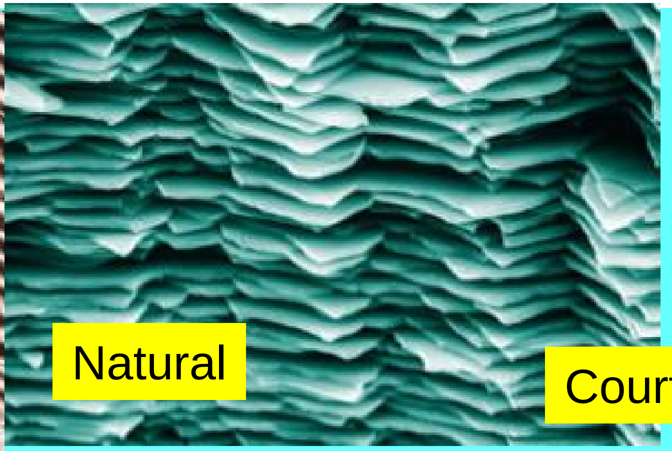

Courtesy of A. Tomasia

Bioinspired Self-Healing

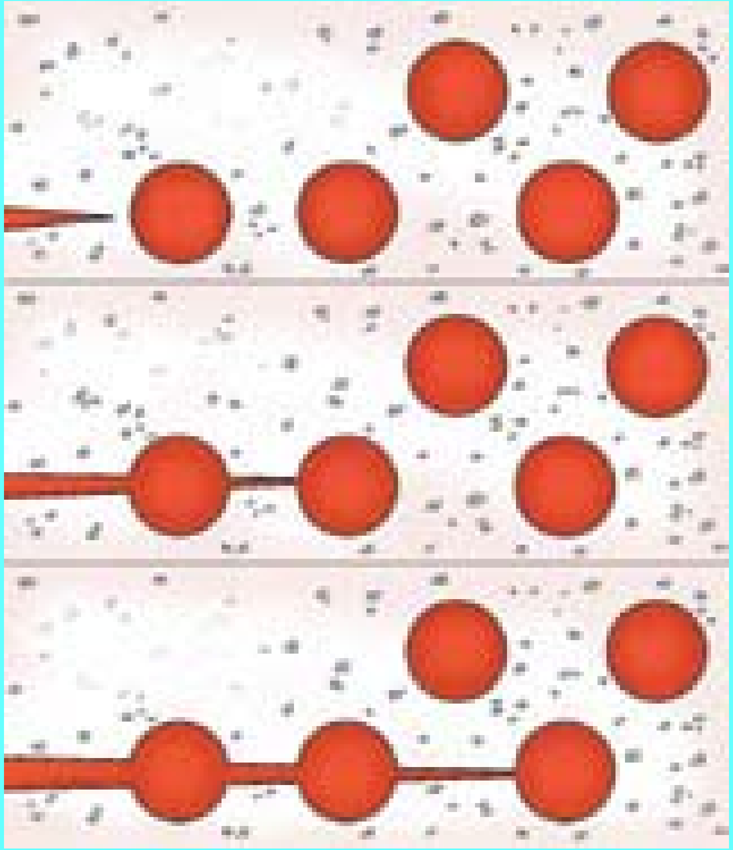

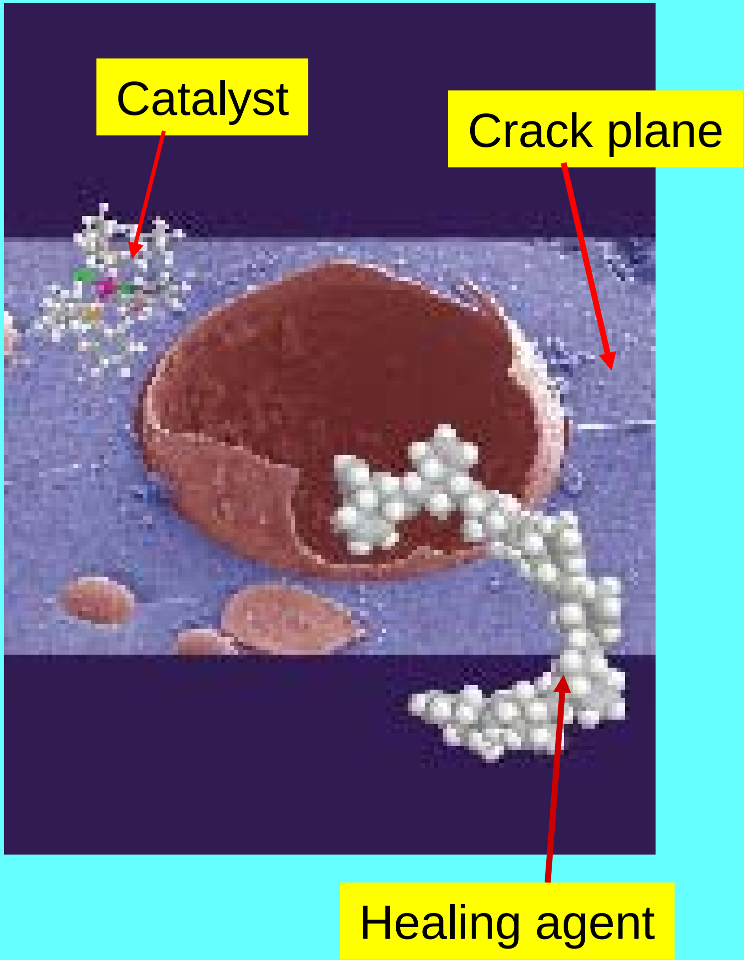

Courtesy of Nancy Sottos
University of Illinois

In the future the healing
materials will be delivered after damage is sensed.